

## Article

# Testing Tectonostratigraphic Hypotheses of the Blountian Phase of the Taconic Orogeny in the Southern Appalachians through an Integrated Geochronological and Sedimentological Study of Ordovician K-Bentonites and Quartz Arenites

Achim D. Herrmann <sup>1,2,\*</sup>, John T. Haynes <sup>3</sup> , Richard Robinet <sup>1,2</sup>, Peter D. Clift <sup>1,2</sup> and Keith E. Goggin <sup>4</sup><sup>1</sup> Department of Geology & Geophysics, Louisiana State University, Baton Rouge, LA 70803, USA<sup>2</sup> Coastal Studies Institute, Louisiana State University, Baton Rouge, LA 70803, USA<sup>3</sup> Department of Geology and Environmental Science, James Madison University, MSC 6903, Harrisonburg, VA 22807, USA; haynesjx@jmu.edu<sup>4</sup> 810 Bent Knoll Ct., Sugar Land, TX 77479, USA

\* Correspondence: aherrmann@lsu.edu

**Abstract:** The tectonic setting of the southernmost part of the eastern margin of Laurentia during the Blountian tectophase (~472–452 Ma) of the Ordovician Taconic Orogeny remains unresolved. Tephra produced by explosive volcanism during this early phase of the orogeny are now K-bentonites, and in many locations, they are interbedded with mature to supermature quartz arenites. We conducted U-Pb analyses of detrital zircons from the sandstones, and of zoned magmatic zircons from the K-bentonites, to constrain the tectonostratigraphic setting with more precision. We also used geochemical fingerprinting of apatite phenocrysts to correlate the K-bentonites in these sandstones along the tectonic front, and we then integrated these results with a depositional systems study of the quartz arenites to further constrain and test competing models of the regional tectonomagmatic setting during that time. The general dearth of detrital zircons that have ages contemporaneous with the volcanic activity, coupled with the predominantly Precambrian ages of the zircons in these Lower Paleozoic quartz arenites that otherwise lack volcanoclastic components—such as detrital VRFs or a muddy matrix derived from an eroding volcanic arc—suggests that magmatic zircons from the tephra layers entered the depositional system only occasionally, and that the volcanic centers were separated geographically from where these quartzose sands were being deposited. Our findings support a tectonostratigraphic and tectonomagmatic model analogous to a combination of select modern settings in the western Pacific and Indonesia, specifically (1) New Guinea, where mature quartz arenites occur in the Cenozoic foreland succession, and (2) Sumatra, where the enormous Toba caldera formed in association with subduction beneath the Cretaceous-aged continental crust of Sumatra.

**Keywords:** Sandbian; Katian; zircon geochronology; apatite geochemistry; tephrochronology; tectonostratigraphy; inherited cores; tephra; Deicke; Millbrig



**Citation:** Herrmann, A.D.; Haynes, J.T.; Robinet, R.; Clift, P.D.; Goggin, K.E. Testing Tectonostratigraphic Hypotheses of the Blountian Phase of the Taconic Orogeny in the Southern Appalachians through an Integrated Geochronological and Sedimentological Study of Ordovician K-Bentonites and Quartz Arenites. *Minerals* **2023**, *13*, 807. <https://doi.org/10.3390/min13060807>

Academic Editor: Paul Alexandre

Received: 1 April 2023

Revised: 19 May 2023

Accepted: 1 June 2023

Published: 13 June 2023



**Copyright:** © 2023 by the authors. Licensee MDPI, Basel, Switzerland. This article is an open access article distributed under the terms and conditions of the Creative Commons Attribution (CC BY) license (<https://creativecommons.org/licenses/by/4.0/>).

## 1. Introduction and Background

Many details of the tectonostratigraphic evolution of the southern Appalachians during the initial part of the Taconic Orogeny (Ordovician, Sandbian to Katian), known generally as the Blount or Blountian phase of the orogeny [1], are still poorly understood. The tectonic setting and tectonic evolution of the northern and north-central parts of the Taconic orogeny have, by comparison, been largely resolved. To explain the Taconic Orogeny in that area (southern Pennsylvania and Maryland to Newfoundland), it is postulated that a volcanic island arc formed above a subduction zone along the eastern margin of the Laurentian continent. This volcanic island arc system then collided with the Laurentian

margin (Figure 1) during the later Ordovician [2,3], causing the early stages of mountain building during the Taconic Orogeny (Figure 2A).

Whereas general consensus exists about the tectonostratigraphic evolution of the northern part of the Taconic Orogen during different phases of the orogeny [4–11], there is still much controversy about the particulars of a workable model that best fits the evidence accumulated from decades of study in the southern part (Figure 1).

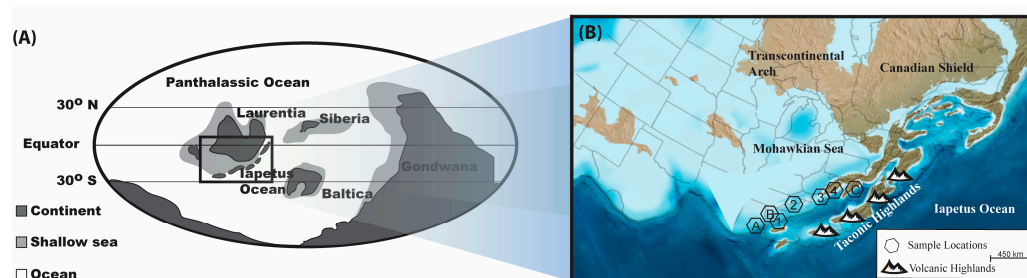


**Figure 1.** (A) Global paleogeography during the Late Ordovician and (B) regional paleogeography with Taconic highlands, associated foreland basin, and sample locations, modified from [12]. Sample locations include (1) Horseleg Mountain, GA (34.22755° N 85.24566° W); (2) Dodson Mountain, TN (36.34248° N 82.95024° W); (3) Crockett Cove, VA (36.99218° N 81.07780° W); (4) Gap Mountain, VA (37.25268° N 80.60900° W). Additional locations (A) Alexander Gap, AL (33.90011° N 85.91659° W); (B) Dirtseller Mountain, AL (34.26946° N 85.61204° W); and (C) Hanging Rock, WV (37.56355° N 80.41196° W) are from [13].

Now, however, recent detailed stratigraphic field studies and petrological and geochemical investigations of the Deicke and Millbrig K-bentonite beds [14–18] in the southern Appalachians have presented compelling evidence that challenges the applicability of the northern Appalachian model to this region. The Deicke K-bentonite ( $454.5 \pm 0.5$  Ma) and the Millbrig K-bentonite ( $452.86 \pm 0.29$ ) [19,20] are the two thickest and most widespread of the many altered tephras that accumulated in the molasse sequence of the Blount foredeep adjacent to the tectonic highlands, and they are estimated to have been deposited over an area of at least  $600,000 \text{ km}^2$  [21]. These tephras (now altered to K-bentonites) and their enclosing strata are exposed in the Valley and Ridge province from Alabama to Virginia, an extensive area of regionally deformed successions of sedimentary strata that comprises the Appalachian fold and thrust belt.

The major explosive eruptions that generated these tephras are likely to have been ultra-Plinian in character. In terms of ash volume, these Paleozoic eruptions were larger than the historic Tambora (1815) and Toba (75 ka) eruptions, and if they were not the largest eruptions of the Phanerozoic, they were probably among the largest [14,17,22]. Enormous explosive eruptions like those in the Ordovician that generated these K-bentonites are typically sourced by rhyolitic to dacitic magmas, rather than by andesitic or basaltic magmas [18]. The trace element geochemistry indicates that there must have been a substantial amount of continental crust that was incorporated during magma generation and subsequent evolution of the source magmas [17]. This tectonomagmatic setting would require that the associated magmatic processes be spatially and genetically linked to continental crust being partially assimilated at that time [23].

By contrast, other studies in the region have been focused on geologic relations in crystalline rock sequences now exposed in the Blue Ridge and Piedmont provinces of Alabama, Georgia, and the Carolinas [24–26]. Those studies proposed an alternate model centered on a back-arc basin system, similar to the Sea of Japan today, whereby the region that comprised the south end of the Taconic Orogen was part of a retroarc basin rather than a foreland basin. In particular, this alternative model hypothesizes that the Blount foredeep developed next to a back-arc basin that developed during deformation associated with tectonic activity along a subduction zone (Figure 2). Because this alternate model requires that a switch in polarity also occurred, i.e., from east-dipping subduction in the north to

west-dipping subduction in the south, its proponents also hypothesize that a transform boundary existed between the northern and southern parts of the Taconic Orogen [24–26].

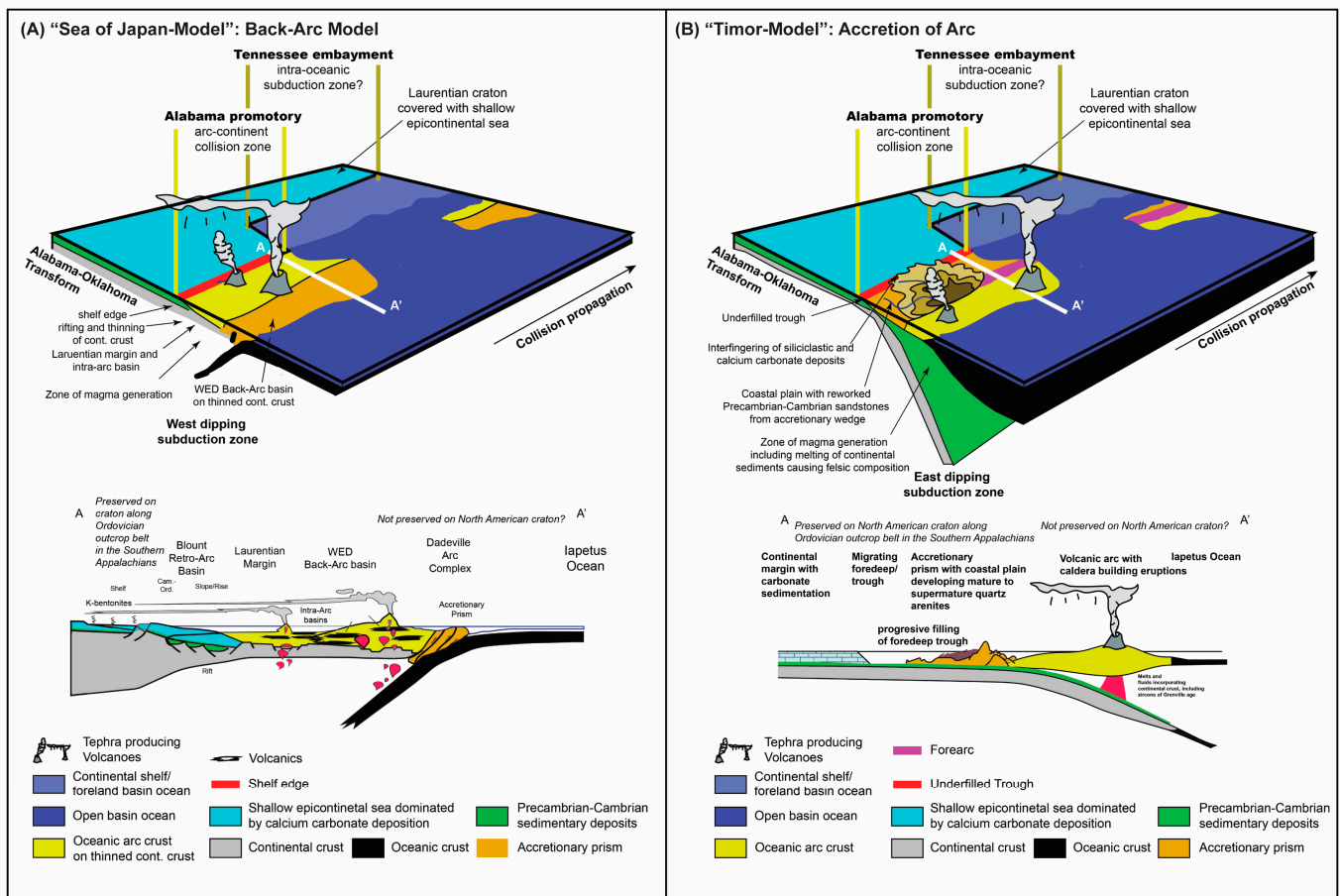


**Figure 2.** Two of the several models, with lithospheric-scale cross sections, previously proposed for the tectonic setting that produced the explosive volcanism that produced the parent tephra of the Deicke and the Millbrig K-bentonite beds. (A) Model of Tull and colleagues [24,26–28]. This model compares to the modern tectonic setting of the Sea of Japan and suggests that the volcanic activity was linked to a continental back-arc setting along the continental margin of Laurentia. (B) Model of Shanmugam and Lash [29], Brookfield and Brett [30], Knight et al. [31], and Mussman and Read [32]. In this model of the Laurentian/arc–continent collision, the outer edge of the passive margin of Laurentia begins to subduct toward the south, and then contractional deformation and thickening of bulldozed passive-margin strata with associated underthrusting of Laurentian continental basement lead to the emergence of an accretionary wedge that forms a subaerial high. This pre-collision accretionary complex sources detritus that is transported toward the volcanic arc, as well as toward the craton, with weathering and erosion in a humid climate and transport and storage of the sediment in floodplains and coastal plains leading to formation of mature quartz arenites that enter the foredeep and interfinger with the muddier molasse sediments at various times.

Here, we report the results of U-Pb geochronology measured on detrital zircon grains extracted from Upper Ordovician pebbly quartz arenites in Alabama, Georgia, Tennessee, West Virginia, and Virginia. These are sandstones with which the Deicke and Millbrig K-bentonites are closely associated stratigraphically, and these K-bentonites and pebbly arenites are themselves part of a thicker and more extensive sequence of red molasse mudrocks (Figure 3). We show how these new data, in tandem with field observations and petrographic analysis of thin sections, help to identify and constrain the provenance of these sands with greater precision. In turn, we show how these data are improving our

understanding of the Blount foreland basin as it evolved over time throughout what is today a multi-state area of the southern Appalachians.

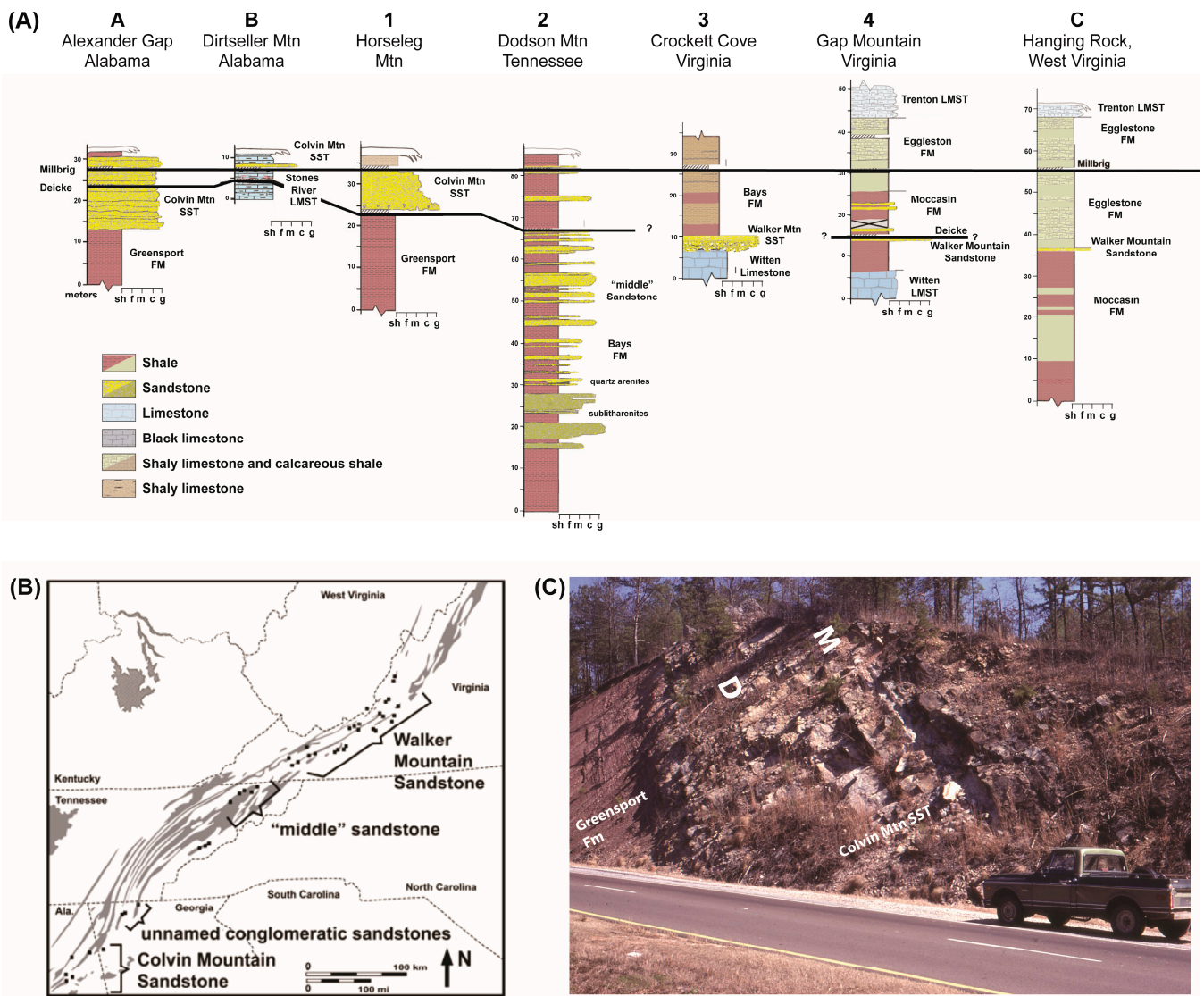


**Figure 3.** (A) Correlation of pebbly arenites and the associated Deicke and Millbrig K-bentonites along strike from Alabama to Virginia; thicknesses in meters. Numbers and letters of outcrops correspond with location identifiers in Figure 1B. Adapted and modified from Herrmann and Haynes [33]. (B) Outcrops of Ordovician quartz arenites, pebbly sandstones, red mudrocks, and associated K-bentonites in the Late Ordovician Blount molasse from Alabama to Virginia, with changes in the associated stratigraphic nomenclature shown. (C) A continuous exposure of the red beds of the Greensport Formation and the overlying quartz arenites of the Colvin Mountain Sandstone (photograph by JT Haynes, March 1986); D—Deicke K-bentonite, M—Millbrig K-bentonite. Alexander Gap, Alabama, bedding top to right.

## 2. Materials and Methods

### 2.1. Sampling

Because the Deicke and Millbrig K-bentonites are altered airfall tephtras, they have widely recognized value as isochrons, or equivalent time horizons, and they are therefore important marker beds in all high-resolution lithostratigraphic correlations between exposures of Sandbian and Katian strata in the Valley and Ridge. Because we have long suspected that the Millbrig K-bentonite bed is present in more of the studied sections of the

molasse sequence red beds than the Deicke K-bentonite, accurate recognition and identification of the Millbrig is especially important; regardless, the Deicke and Millbrig K-bentonites are the only isochrons as yet known that can be used to support high-resolution correlation of the several sections along the outcrop belt in the southern Appalachians from Virginia south to Alabama [14,15,33,34].

Ordovician quartz arenites were collected from seven localities in the Blount foredeep sequence along a NE–SW transect in the southern Appalachians (Figures 1 and 3). The Alexander Gap, Dirtseller Mountain, Horseleg Mountain, Dodson Mountain, Crockett Cove, and Hanging Rock samples were disaggregated using a selfrag machine, and the Gap Mountain samples were broken and crushed at JMU. Samples were placed in a 5% HCl bath and then put through a 38-micron testing sieve, followed by density separation using lithium metatungstate at a density of  $\sim 2.8 \text{ g/cm}^3$ . Zircons were picked from the heavy mineral separates using a bifocal microscope and then mounted in a cold-setting resin and subsequently polished to expose the zircon grains. Grain size and sampling biases are of great concern for detrital zircon record interpretations [35]. Analyzing two different sandstone samples from the Horseleg Mountain location yielded no major differences in age distribution (see Table 2 in [13]). No grain size analyses were performed. U-Pb ages are available in Supplementary Material Table S1.

## 2.2. Apatite Phenocryst “Fingerprinting” Using Laser Ablation Inductively Coupled Plasma Mass Spectrometry (LA-ICP-MS)

Geochemistry of apatite phenocrysts from Ordovician K-bentonites is a valuable tephrochronology tool [12,36,37]. Because the Deicke and Millbrig K-bentonites occur within mature quartz arenites at several of the exposures, we sampled those two K-bentonite beds at several locations as well, so as to confirm that a specific K-bentonite bed is in fact accurately identified using the unique geochemistry of apatites from individual eruptive events. These samples were immersed in deionized water and allowed to disaggregate, and then they were sieved and separated into coarse and fine grain fractions using a combination of 841  $\mu\text{m}$ , 125  $\mu\text{m}$ , and 63  $\mu\text{m}$  sieves. The sediments collected in the 125  $\mu\text{m}$  sieve were dried overnight at 50 °C, and these dried samples were further separated into higher-density and lower-density portions using sodium polytungstate, again at a density of  $\sim 2.8 \text{ g/cm}^3$ . After gravity separation, apatite phenocrysts were hand-picked using a binocular microscope and a fine-bristled paint brush and then mounted on a glass plate using double-sided tape and cast in epoxy in preparation for geochemical analysis.

Details on analytical conditions for the geochemical analysis of apatite phenocrysts from the K-bentonite beds are shown in Table 1. Isotopes of elements analyzed included  $^{24}\text{Mg}$  (dw = 0.03),  $^{43}\text{Ca}$  (dw = 0.01),  $^{55}\text{Mn}$  (dw = 0.01),  $^{57}\text{Fe}$  (dw = 0.01),  $^{89}\text{Y}$  (dw = 0.01),  $^{232}\text{Th}$  (dw = 0.01),  $^{238}\text{U}$  (dw = 0.01), and the lanthanide series (REE; dw = 0.01). Element concentrations were normalized against NIST-612 glass (8.5 wt.% Ca). Laser energy could not be measured due to a lack of an energy meter and precise crater size measurements but is estimated to be in the range of commonly used energy fluence according to the manufacturer. Pre-ablation laser delay was 10 s and washout times were 30 s in all experiments. There are no internationally accepted apatite standards for LA-ICP-MS, so a combination of three in-house apatite standards (Durango, Blue Brazil, and Smithsonian NMNH 104021) was used to monitor instrument precision. Supplementary Material Table S2 includes statistical data for these standards. Igor Pro with Iolite software was used for data reduction [38], with  $^{43}\text{Ca}$  used as the internal element standard with a stoichiometric Ca content for apatite.

**Table 1.** Laser ablation parameters used.

	Zircons		Apatites	
Spot Size	25 $\mu\text{m}$	10 $\mu\text{m}$	25 $\mu\text{m}$	50 $\mu\text{m}$
Laser Energy	10%	50%	30%	30%
Frequency	20 Hz	20 Hz	10 Hz	10 Hz
Shutter Delay	10 s	10 s	10 s	10 s
Burst Count	700	700	800	600
He Gas Flow	~600 mL/min	~600 mL/min	~700 mL/min	~650 mL/min

### 2.3. U-Pb Geochronology Using Laser Ablation Inductively Coupled Plasma Mass Spectrometry (LA-ICP-MS)

U-Pb geochronology was performed using a CETAC Technologies LSX-213 G2 laser ablation system connected to a Thermo Scientific iCAP Q-ICP-MS in the Department of Geology and Geophysics at LSU. Helium gas was used for transporting ablated aerosol from the ablation chamber, with argon being added just prior to the ICP-MS torch as an additional carrier gas. The following isotopes were measured:  $^{91}\text{Zr}$  ( $dw = 0.01$ ),  $^{202}\text{Hg}$ ,  $^{204}\text{Pb}/\text{Hg}$  ( $dw = 0.01$ ),  $^{206}\text{Pb}$  ( $dw = 0.01$ ),  $^{207}\text{Pb}$  ( $dw = 0.01$ ),  $^{208}\text{Pb}$  ( $dw = 0.01$ ),  $^{232}\text{Th}$  ( $dw = 0.01$ ), and  $^{238}\text{U}$  ( $dw = 0.01$ ).  $^{235}\text{U}$  was not measured, and  $^{207}\text{Pb}/^{235}\text{U}$  ages were calculated using a ratio of 137.8180. Laser energy could not be measured due to a lack of an energy meter and precise crater size measurements but is estimated to be in the range of commonly used energy fluence according to the manufacturer. Pre-ablation laser delay was 10 s and washout times were 30 s in all experiments.

The runs were calibrated using the 91500 zircon standard ( $1063.51 \pm 0.39$  Ma; [39,40]) as the external calibration standard. Temora2 ( $416.78 \pm 0.33$  Ma; [41]) and Plesovice ( $337.15$  Ma; [40,42]) were used as secondary standards to evaluate the accuracy and precision of the analyses; all standards were ablated before, during, and after all runs to monitor analytical precision and possible instrument drift and to calibrate ages. Temora2 had a precision and accuracy of  $413.04 \pm 1.66$  Ma ( $n = 104$ ) for the duration of the study, while Plesovice had a precision and accuracy of  $337.44 \pm 2.07$  Ma ( $n = 32$ ). Magmatic zircon data were reduced with the Wavemetrics Igor Pro software (v. 6.37) and Iolite (v. 2.5) as an add-in [38]. After data reduction, all U-Pb ages were plotted as kernel density estimation (KDE) plots. Detrital zircons' raw data were reduced using the VizualAge module [43] within Iolite 4 [44]. All ages reported herein are less than 20% discordant. Zircon age data for the Alexander Gap, Dirtseller Mountain, and Hanging Rock locations were taken from [13], and analytical details for those analyses can be obtained from there.

## 3. Results

### 3.1. K-Bentonite Apatite Geochemistry

Analyses of the apatite phenocryst data comparing Fe vs. Mn vs. Mg concentrations, and Mg vs. La/Tb vs. Ce/Tb concentrations, reveal two dominant clusters of Millbrig apatites, with the first cluster centered around 600 ppm Fe, 900 ppm Mn, and 250 ppm Mg and the second cluster centered around 800 ppm Fe, 755 ppm Mn, and 405 ppm Mg, and a single cluster of Deicke apatites centered around 700 ppm Fe, 450 ppm Mn, and 750 ppm Mg (Figure 4).

### 3.2. U-Pb Geochemistry, and Fabric of Zircons with Magmatic Rims of Taconic Age

Many of the detrital zircon grains have older—and commonly rounded—zircon cores encased by visibly zoned magmatic rims (Figure 5). These different domains have distinct age differences, with the inherited cores having ages as old as 1.2 Ga, whereas the ages of the zoned rims are less than 700 Ma, with several that are as young as the widely accepted radiometric ages of the Deicke and Millbrig K-bentonites (Figure 5).

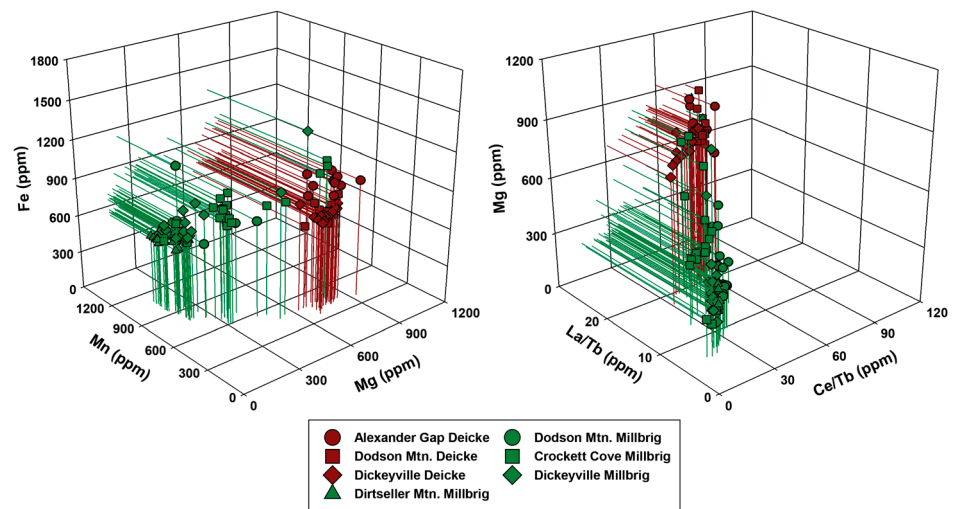


**Figure 4.** Geochemical fingerprinting of apatite phenocrysts in suspected Deicke and Millbrig K-bentonite samples where they are associated with the Ordovician quartz arenites. For comparison, analyses of apatite phenocrysts in the Deicke and Millbrig K-bentonites from Dickeyville, Wisconsin (Upper Mississippi Valley), are also plotted. Uncertainties for measurements are  $\pm 10\%$ .

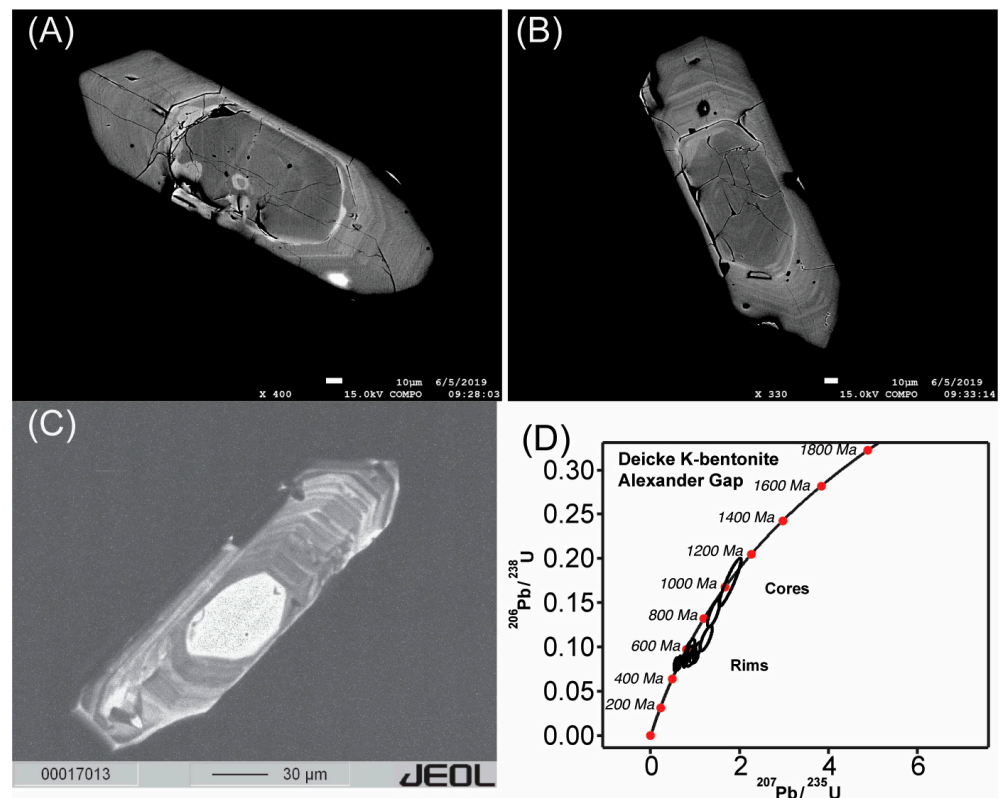


**Figure 5.** (A,B) Backscattered electron (BSE) and (C) cathodoluminescence (CL) images from select magmatic zircon grains from the Deicke K-bentonite at Alexander Gap, AL. (D) U-Pb results from magmatic rims and cores from zircons at Alexander Gap.

### 3.3. U-Pb Geochemistry of Detrital Zircons

The majority of the detrital zircons in the quartz arenites, with the exception of the sample from Dirtseller Mountain, have  $^{207}\text{Pb}/^{235}\text{U}$  ages of 900–1200 Ma (Figure 6). Because the Colvin Mountain Sandstone directly overlies the Millbrig K-bentonite at the Dirtseller Mountain exposure (Figures 3 and 6), the presence of several detrital zircon grains in

the sandstone from there that are younger than the Millbrig is to be expected, given this stratigraphic relationship.

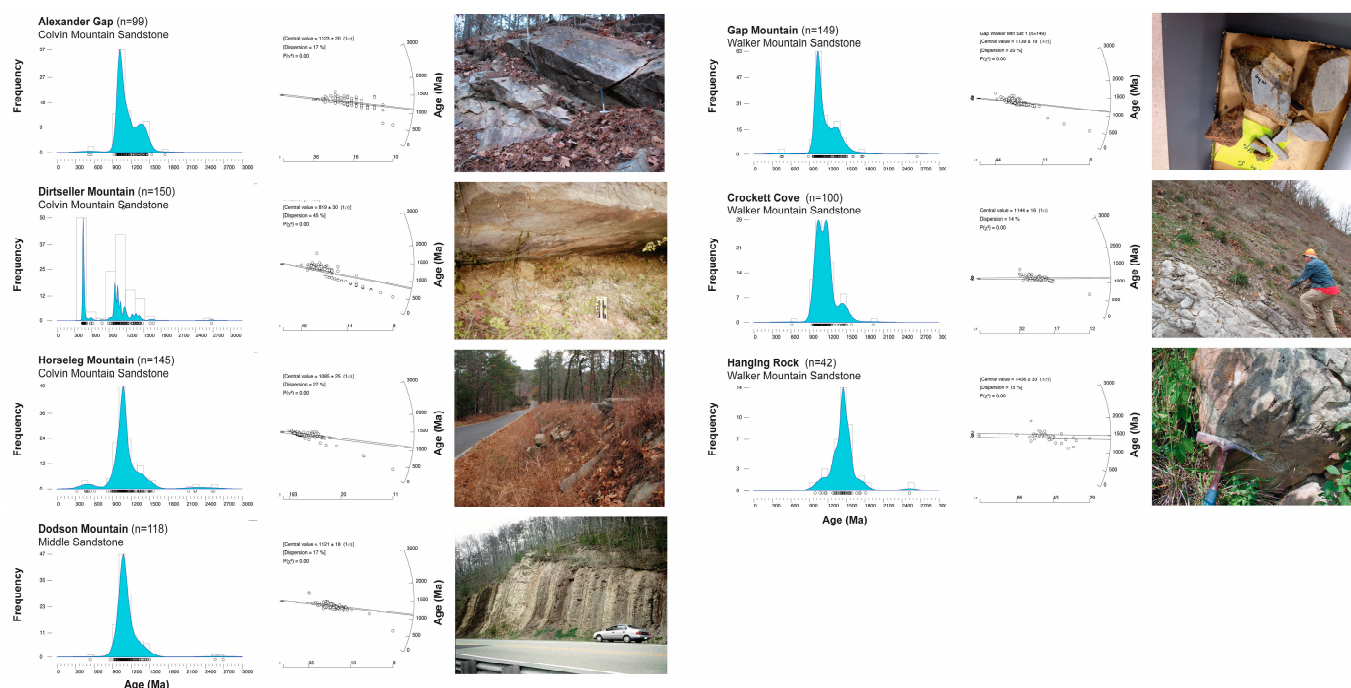


**Figure 6.** KDE plots and radial plots showing U-Pb ages for detrital zircons. Also shown are representative pictures of outcrops or hand samples of sandstones, and at Alexander Gap, Dirtseller Mountain, Horseleg Mountain, and Dodson Mountain, of associated K-bentonite beds as well [14,34]. Letters and numbers are the same as those in Figures 1 and 3.

## 4. Discussion

### 4.1. Apatite Geochemistry-Based High-Resolution Correlation of K-Bentonites

Mg and Mn concentrations in apatite phenocrysts have proven to be two of the best discriminator elements for identifying and “fingerprinting” Ordovician K-bentonites for correlation purposes [36,45]. Although there is some scatter, the clustering of our data obtained from analyses of apatite phenocrysts confirm that the Deicke and Millbrig K-bentonite beds are each present in—and thus stratigraphically associated with—some or all of these mature quartz arenites in the molasse red bed sequence. Specifically, our geochemical “fingerprinting” confirms the presence of the Deicke and Millbrig K-bentonites at Dodson Mountain and the presence of the Millbrig K-bentonite at Dirtseller Mountain and Alexander Gap, which were suggested by prior work based on different mineralogical criteria [14,33,34]. The heavy mineral separates from the Deicke K-bentonite at Alexander Gap and at Horseleg Mountain, identified previously on the basis of its ilmenite phenocrysts [14,33], did not contain apatite, and thus that sample could not be geochemically fingerprinted. Although we did not collect any K-bentonite samples at Crockett Cove or Gap Mountain for this study, we have previously identified the Millbrig in both sections on the basis of mineralogical and stratigraphic evidence [14,15,34].

### 4.2. Tectonostratigraphic Constraints Based on the Texture and U-Pb Geochronology of Magmatic Zircons with Taconic Ages

In several young volcanic arc settings, old inherited cores in magmatic zircons are known to occur [46–49]. That is a finding which shows that the presence of old, Grenville-aged inherited cores in the detrital zircons of the Ordovician quartz arenites can help to constrain the tectonic and depositional settings of those sandstones, because where the melting occurred within the subduction zone, a source of preexisting zircon grains must unambiguously have been present in the country rock being assimilated and melted. These

zircons could have originated from within the overriding plate, but that is not a necessary requirement because Aitchison et al. [50] showed that zircon and rutile can be transferred from the subducting slab to the overlying wedge. Thus, the transfer of material in such settings is not limited to fluids, but in fact, these minerals can then be incorporated into ascending magmas as xenocrystic mineral grains in a subduction zone. In addition to the zircons from the Deicke K-bentonite that have inherited cores, zircon cores from detrital zircons also have significant internal age differences; some rims of magmatic and detrital zircons are Taconic in age ( $450 \pm 15$  Ma and  $466 \pm 16$  Ma;  $2\sigma$ ), whereas the inherited cores have ages that align them with zircons derived from the Grenville/Keweenawan ( $1061 \pm 39$  Ma;  $2\sigma$ ) and Yavapai–Mazatzal ( $1663 \pm 30$  Ma;  $2\sigma$ ) provinces.

Inherited cores in zircons from the Deicke K-bentonite were noted by Samson et al. [51], who suggested that the Deicke and other K-bentonites, instead of being derived from mantle-sourced primitive melts as expected in a young island arc setting, were influenced instead by melting of evolved continental crust. In their model, a volcanic arc had formed atop the Proterozoic continental crust that was itself also above colliding and underthrusting subducting continental crust.

More recently, Herrmann et al. [37] showed that the geochemistry of magmatic apatite and zircon phenocrysts from the Deicke K-bentonite—and of melt inclusions in those phenocrysts—is consistent with an arc–trench subduction system where subduction of older sedimentary rocks resulted in their subsequently being incorporated into the melt during or prior to collision. Specifically, these authors showed that the trace-metal geochemistry of these Taconic-age rims on these zircons (e.g., Sc, Y, Nb concentrations) is indicative of a melt that was associated with continental crustal melt with a high level of differentiation, rather than a melt that was mantle-derived or strongly mantle-influenced. Our textural and U-Pb geochronological data obtained from analyses of detrital and magmatic zircons with Taconic ages from the quartz arenites support this model.

#### 4.3. Sedimentology of Ordovician Arenites, and Their Stratigraphic Relationships with the K-Bentonites

In the red beds of the molasse sequence that occur from west-central Virginia to central Alabama [14,22,23], the Ordovician Deicke and Millbrig K-bentonites occur in close stratigraphic association with several quartz arenites (Figure 3). Standard collisional tectonic models show molasse sediments consisting of fine to coarse continental clastic sedimentary rocks being derived from eroding tectonic highlands and then deposited in an adjacent foreland basin during later stages of orogenic activity [52], when waning tectonism is accompanied by a decline in explosive volcanism like that which was responsible for the tephra that are now the K-bentonites. The molasse sediments that accumulated as the Blountian tectophase was ending include red mudrocks (Figure 3) of the Moccasin, Bays, and Greensport formations [53], as well as the distinctive sandy to pebbly quartz arenites [15,33,54–56].

These sandstones and conglomerates have a variety of ichnofossils (Figure 7) including *Skolithos* sp. burrows, some of which exceed 60 cm in length, as well as dense horizontal burrows that likely are some combination of *Planolites* sp., *Scoyenia* sp., *Arenicolites* sp., and *Trypanites* sp. Common sedimentary structures (Figure 8) include trough and tabular cross-bedding, low-angle cross-bedding, tidal bundles, scour-and-fill structures, normal and reverse grading, and planar lamination. Other structures including oscillation ripples, adhesion ripples, and slightly overturned and oversteepened ripple cross-laminations range from being far less common to only a single known occurrence. Collectively, these ichnofossils and sedimentary structures point to deposition in environments that included wave-dominated tidal flats/tidal channels, beaches and dunes, nearshore bars, and fluvial-to tidal-dominated deltas and associated lagoons and estuaries [15,33,34,54–64].

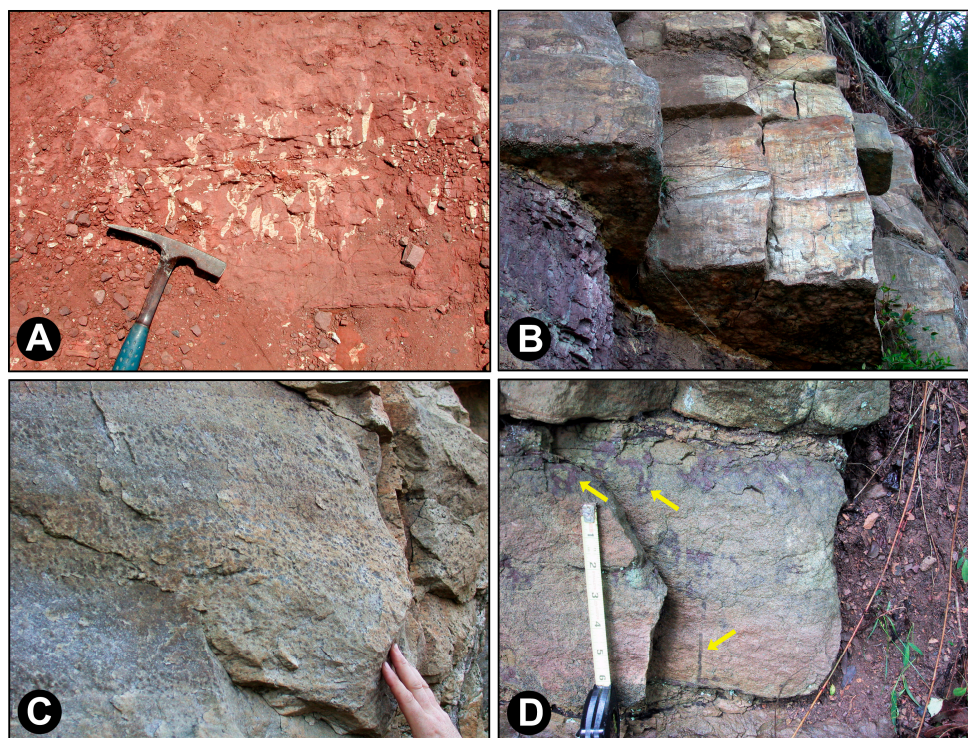


**Figure 7.** Ichnofossils in the quartz arenites and red beds of the Blount molasse (A) *Trypanites?* burrows in red beds of the Bays Formation near Dalton, Georgia. (B) *Skolithos* burrows exceeding 60 cm in length in the “middle” sandstone member. Bays Mountain Park, Tennessee. (C) Abundant *Planolites?* burrows in the “middle” sandstone. Bays Mountain Park, Tennessee. (D) *Trypanites?* and *Scoyenia?* burrows (upper arrows) outlined by red iron oxide in the “middle” sandstone with a *Skolithos* burrow (lower arrow) at the base of the bed. Bays Mountain Park, Tennessee.

These sands and pebbly gravels were sourced from one or more terranes in the Taconic highlands where older passive margin sedimentary rocks, low-rank metamorphic quartzites and hydrothermally altered sequences, higher-rank regionally metamorphosed phyllites and schists, and some plutonic igneous or very-high-rank metamorphic gneisses collectively were exposed. Weathering and erosion of these source rocks ultimately produced the distinctive framework grains of sedimentary and metamorphic rock fragments (SRFs, MRFs) seen in thin sections. Observed MRFs include amphibolite, tourmaline schist (Figure 9A), unstretched, stretched, and sutured polycrystalline quartz (Figure 9D–F), and vein quartz with inclusions of vermicular chlorite and specular hematite (Figure 9C). SRFs include siltstone, oolitic/peloidal/bioclastic limestone (Figure 9B,H), and shell fragments (Figure 9K), as well as abundant chert of many types including structureless black, gray, and white chert, silicified oolitic grainstone, silicified peloidal grainstone, hematitic chert (jasper), and banded agate from silicified paleosols including chalcedony with cubic zoning that is pseudomorphic after halite casts. In some samples, a minor plagioclase component in the framework grain population (Figure 9F) points to a contribution from igneous rocks—likely plutonic—given that a few quartzo-feldspathic rock fragments (QFRFs) are present (Figure 9D), but there is a complete lack of volcanic rock fragments (VRFs) [15,33,54,55,65].

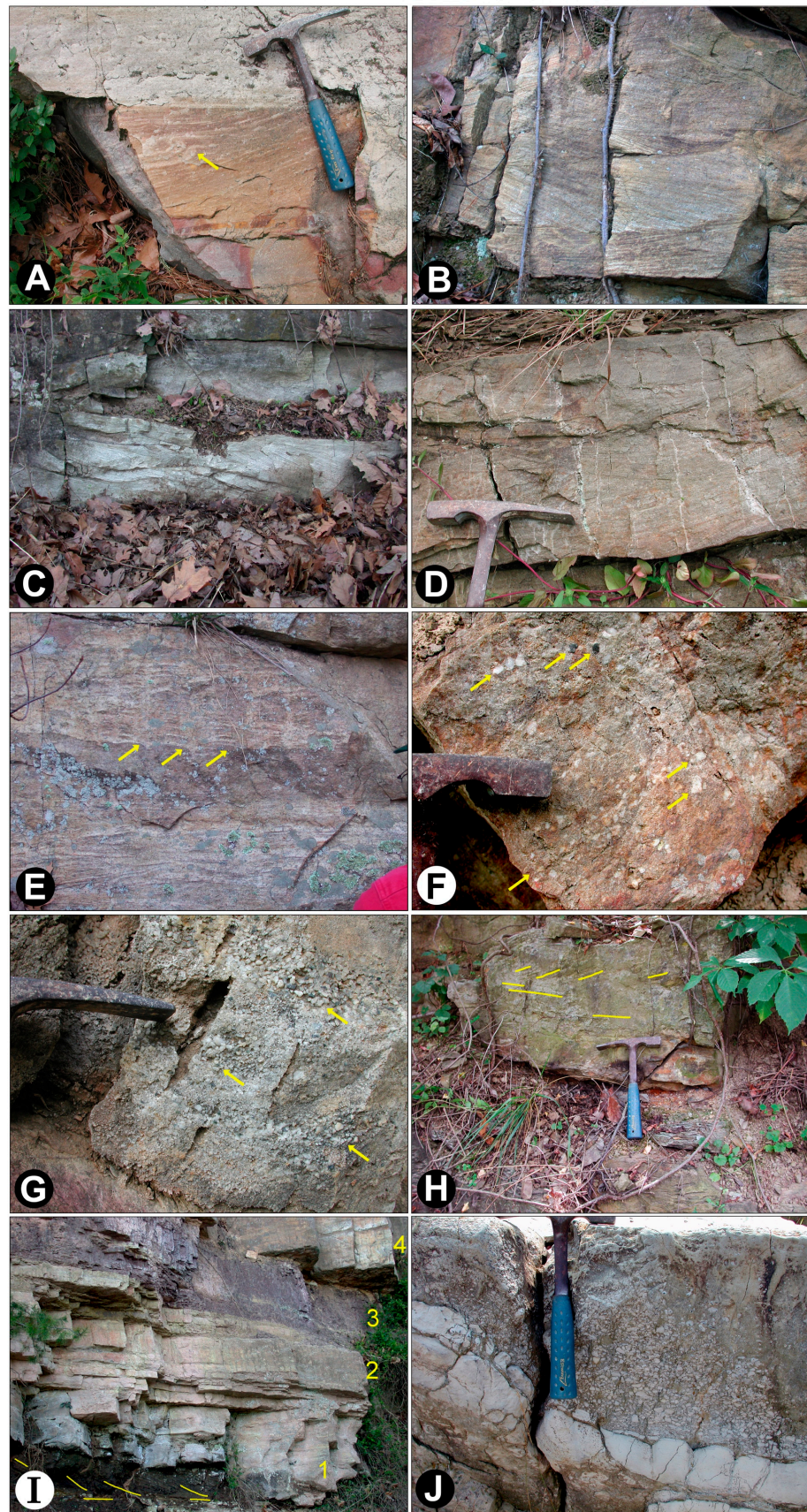


**Figure 8.** Sedimentary structures in the quartz arenites and associated strata of the Blount molasse. (A) Oversteepened and overturned crests (arrow) outlined by ripple laminae in a cross-bed set in the Colvin Mountain Sandstone, Alexander Gap, Alabama. (B) Planar cross-bedding in the “middle”

sandstone. Bays Mountain Park, Tennessee. (C) Planar and trough cross-bedding, and tidal bundles, in the “middle” sandstone. Bays Mountain Park, Tennessee. (D) Trough cross-bedding in the Walker Mountain Sandstone. Ellett, Virginia. (E) Convex up laminations (arrows) interpreted as adhesion ripples, which form by wind blowing dry sand across a wet or damp substrate; “middle” sandstone. Bays Mountain Park, Tennessee. (F) Discontinuous lenses of sub-angular to sub-rounded quartz and chert granules and pebbles (arrows) with some indistinct normal and reverse grading in the Walker Mountain Sandstone. Ellett, Virginia (G) Disconformity between red calcareous mudrocks of the Moccasin Formation (lower left) and the overlying Walker Mountain Sandstone with its indistinctly cross-bedded coarse sand and granules and pebbles of rounded quartz (arrows). Goodwins Ferry, Virginia. (H) Disconformity between the dark gray mudrocks of the Liberty Hall Formation (bottom, to hammer) and the overlying Walker Mountain Sandstone with tabular to indistinctly tangential cross-bedding (yellow lines) in the sandstone. Peters Creek, Virginia. (I) Cyclicity in the “middle” sandstone and associated red beds of the Bays Formation; lowest bed (1) is a quartz arenite with tangential cross-bedding that is overlain by a quartz arenite with extensive *Skolithos* burrows (2), which grades upward into a red mudrock—possibly a paleosol—that includes some *Trypanites?* burrows (3) and has a sharp contact with an overlying thick quartz arenite bed that also has extensive *Skolithos* burrows (4). Bays Mountain Park, Tennessee. (J) Disconformable contact (base of hammer) that is part of an ~3 m wide and 2 m deep scour-and-fill structure with discrete channel boundaries between black lime mudstones of the Liberty Hall Limestone and the Bays Formation, with the lower 1–2 m of the Bays consisting of an intraclast (“flat-pebble”) conglomerate comprising locally reworked rounded clasts of the Liberty Hall in a matrix of argillaceous micrite; the Walker Mountain Sandstone is ~1 m upsection, the Deicke K-bentonite is ~2 m upsection, and the Millbrig K-bentonite is ~5 m upsection. Millers Cove, Virginia.

During the time that these sediments were transported toward their final depositional site in the Taconic foredeep, they likely spent appreciable lengths of time in intermittent storage in floodplain alluvium, where extensive weathering destroyed many of the more labile grains, such as feldspars, and left even the more durable grains highly altered (Figure 9D). Eventually, the sands and gravels were transported to coastal areas by wind and by rivers that flowed across the now uplifted and exposed older ramp and basin margin carbonate sediments [54–56]. These in turn contributed more sediment, including detrital zircon grains (Figure 9J). Much—perhaps most—of the sand and gravel accumulated in proximal to distal shelf environments of the now nearly filled Taconic foredeep (Figure 9K,L), but some of the gravels entered deeper waters along the edge of the shelf where they became the submarine fan deposits of the Fincastle Conglomerate, which is located at the northeasternmost margin of the Blount foredeep [54–56]. The red muds and clean quartzose sands did not reach this northernmost edge of the basin as molasse deposits, because the sediment that was transported down the feeder channels of the Fincastle submarine fan system consisted of sands and gravels with lesser non-red mud [66], and to the northeast (present-day) of the Fincastle area, the Taconic foredeep did not fill during the Blountian phase, but instead remained relatively deep in the region of modern West Virginia, Maryland, Pennsylvania, and New York, where much of the Blount-age sequence consists of deep water carbonates, e.g., the Salona Limestone [22,36]. Migrating sand waves produced occasional cross-bedding (Figure 8B–D,H), and episodic reworking by eolian processes produced the distinctive bimodal mature textures [67,68] seen in several samples of the Walker Mountain Sandstone (Figure 9I). Further reworking in nearshore marine to beach environments is indicated by the low-angle swash cross-bedding with normal and reverse grading of coarse sands and gravels (Figure 8) and by the thin beds of shell fragments seen in several samples (Figure 9K) [54,55]. Compositional maturity was enhanced by sorting and washing of the sand by longshore and tidal currents and associated wave action as the sands and gravels were spread across the beveled and disconformable surface (Figure 8G,H,J) that had developed on the youngest units of the older carbonate ramp and basin margin sequence [54–56].

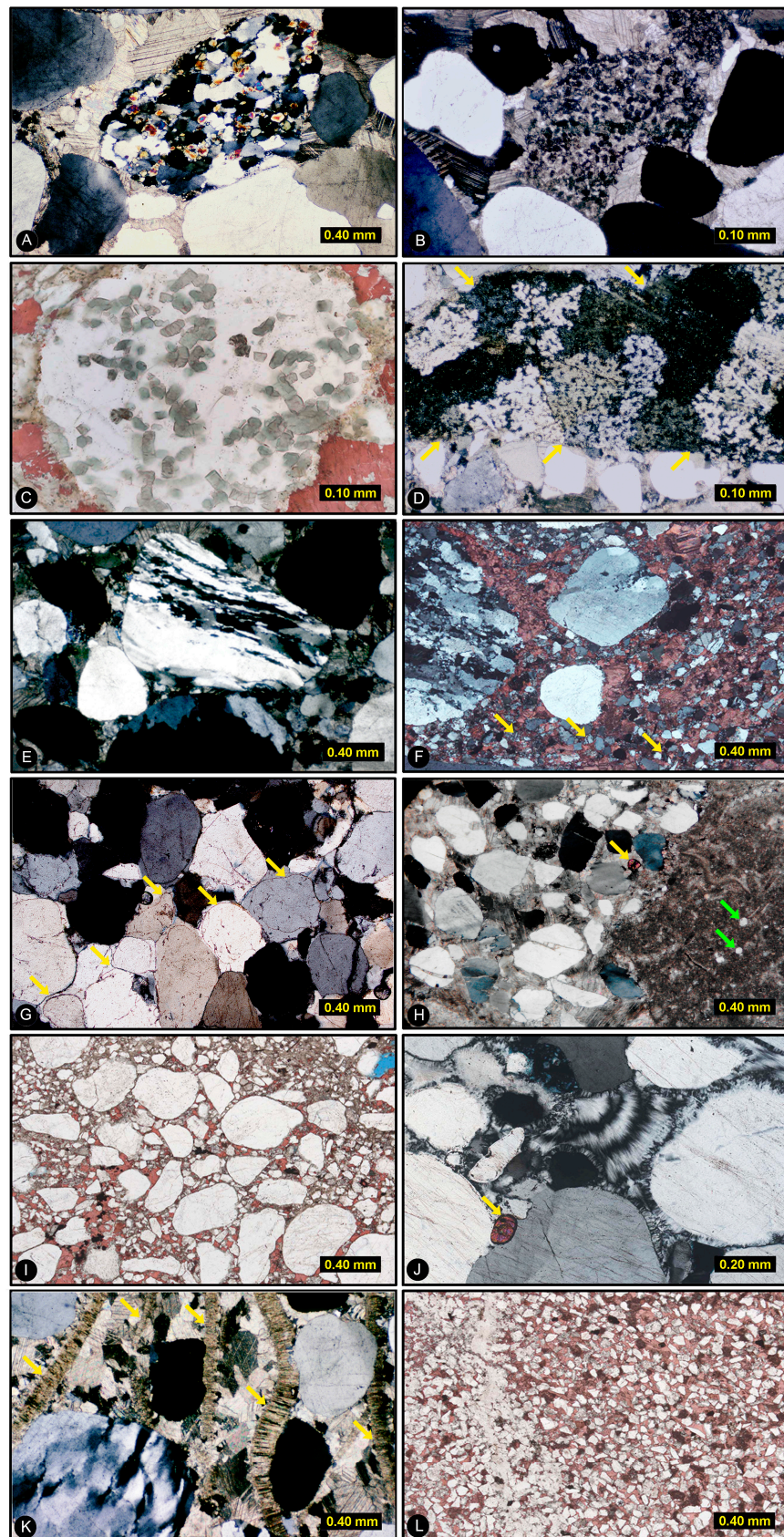


**Figure 9.** Photomicrographs of Ordovician quartz arenites in the Blount molasse; MRF—metamorphic rock fragment, SRF—sedimentary rock fragment, QFRF—quartzofeldspathic rock fragment, PPL—plane-polarized light, XPL—cross-polarized light. Variable scale in each. (A) Sub-rounded

tourmaline schist MRF and surrounding monocrystalline quartz all cemented by non-ferroan calcite. Walker Mountain Sandstone, Newport, Virginia; unstained thin section, XPL. (B) Sub-angular peloidal grainstone SRF with trace quartz silt grains and surrounding monocrystalline quartz all cemented by non-ferroan calcite. Walker Mountain Sandstone, Goodwins Ferry, Virginia; unstained thin section, XPL. (C) Abundant vermicular chlorite inclusions in a sub-rounded vein quartz MRF cemented by non-ferroan calcite. Walker Mountain Sandstone, Trigg, Virginia; stained thin section, PPL. (D) Elongate granule of unstretched polycrystalline quartz grain (grain boundary delineated by arrows) that is internally fractured and has been extensively weathered and pitted but does not have sutured internal crystal boundaries or truly polygonal boundaries; this is probably a plutonic QFRF or possibly a low-rank quartzite MRF that was altered by weathering along its route during extensive residence in alluvial deposits prior to re-mobilization and further travel. Note the smaller unaltered monocrystalline quartz grains surrounding the larger highly altered grain, all cemented by non-ferroan calcite. Walker Mountain Sandstone, Newport, Virginia, unstained thin section, XPL. (E) Sub-rounded grain of stretched polycrystalline quartz showing preferential alignment of the constituent crystals, and sutured and diffuse internal boundaries between composite crystals. This grain, from a high-rank metamorphic terrane, and the surrounding monocrystalline and polycrystalline quartz grains are cemented by non-ferroan calcite. Walker Mountain Sandstone, Newport, Virginia, unstained thin section, XPL. (F) Silt- to very-fine-sand-sized plagioclase framework grains (arrows) in the fine fraction of a bimodal sandstone, all cemented by non-ferroan calcite. Note the monocrystalline and two polycrystalline quartz grains, with the larger one at left displaying marked elongation and some suturing of its internal crystal boundaries, indicative of its metamorphic origin. Walker Mountain Sandstone, Goodwins Ferry, Virginia, stained thin section, XPL. (G) Monocrystalline quartz grains cemented by syntaxial quartz overgrowths which show enhanced visibility because of the “dust rims” (arrows) that mark the contact of the overgrowths with the rounded detrital grain cores. Walker Mountain Sandstone (type section), Keyword Branch, Virginia, unstained thin section, XPL. (H) Sub-angular fossiliferous wackestone SRF at right with small euhedral authigenic quartz crystals (green arrows) that attest to the prior burial and diagenesis of the older limestone from which this SRF was derived. Note the rounded detrital zircon (yellow arrow) and the surrounding quartz grains of various shapes and origins, all cemented by non-ferroan calcite. Walker Mountain Sandstone, Connor Valley, Virginia, unstained thin section, XPL. (I) Prominent bimodal texture of larger and more rounded quartz grains surrounded by smaller and more angular silt to very-fine-sand-sized quartz grains, cemented by non-ferroan calcite and some argillaceous matrix; bimodality is common in many of the quartz arenites of this age, and that texture is interpreted as evidence of eolian reworking of the sand, probably not long before the sediment was moved to its final site of deposition. Colvin Mountain Sandstone, Dirtseller Mountain, Alabama, stained thin section, PPL. (J) Rounded monocrystalline quartz grains and a well-rounded detrital zircon (arrow) cemented by zebraic chalcedony. Colvin Mountain Sandstone, Horseleg Mountain, Georgia, stained thin section, XPL. (K) Shell fragments (arrows) with prominent simple prismatic internal structure enclosed by rounded quartz grains including a stretched polycrystalline quartz granule at lower left, all cemented by non-ferroan calcite. The shells are bivalve (or possibly brachiopod) fragments interpreted as having accumulated in a strand line or as part of storm washover deposits in a nearshore marine to beach environment. Walker Mountain Sandstone, Newport, Virginia, unstained thin section, XPL. (L) Calcareneous quartz arenite comprising sub-angular fine- to very-fine-grained quartz sand and silt (80%–85% of framework grains), and peloids (15%–20% of framework grains), all cemented by non-ferroan calcite. This sample is at the northwestern limit of where the quartz arenite facies can be recognized in the Upper Ordovician of southern Appalachians, and its finer grain size and intermingled carbonate framework grains point to deposition in a carbonate shelf setting punctuated by siliciclastic deposition only by this thin bed of sandstone. Walker Mountain Sandstone, McGraw Gap, Virginia, stained thin section, PPL.

Our prior study of Ordovician mudstone compositions in northern Virginia showed that MgO and total FeO content increases upsection in tandem with an increase in the volume of chlorite, and we interpreted this chemical trend as evidence that, later in the

Ordovician, muds derived from weathering and erosion of a volcanic arc had begun to enter the Taconic basin in that area, which is far beyond the northeastern edge of the Blount foredeep [69]. To date, however, we have found no petrographic evidence that the sand or gravel fractions—vs. the mud fraction—coming into the nearly filled Blount foredeep at this time included detritus derived from an eroding volcanic arc. This conclusion is supported by petrographic comparison [70] of the Sandbian Walker Mountain Sandstone of the Blount molasse with a younger coarse pebbly sandstone in the region, the Katian Oswego Sandstone, which is the oldest unit of the younger Queenston molasse and is associated with the main Taconic tectophase. A QFL plot (Figure 10) of some of the coarsest Walker Mountain Sandstone samples and some of the very coarse to conglomeratic Oswego Sandstone samples shows some overlap in the Recycled Orogenic field, and it is evident that the Oswego Sandstone is a less mature sediment overall, yet it is one that nevertheless contains no evidence of eroded arc material in the sand and gravel fraction. So although mud being eroded from the arc was evidently carried in suspension into the foredeep around or across the accretionary wedge [69], the coarser fractions were being trapped on the arc side of the accretionary prism and thus were kept from entering the foredeep as part of either the Blount molasse or the younger Queenston molasse. Mack [65], finding no VRFs in the framework grain population of sands in the Blount molasse, likewise concluded that the sediment now in the Blount molasse was not derived from a disintegrating volcanic arc. It is noteworthy that in the modern Taiwan arc–continent collision, very little of the sediment being eroded from the island is sourced from the Luzon volcanic arc [71].

The best constraint on the timing of precisely when these quartz-rich sands and gravels began to accumulate in the Blount foredeep is their stratigraphic position relative to the Deicke and the Millbrig K-bentonites, because as noted above, those beds are altered tephra and thus are isochronous event beds whose relationship to the coarse sands and gravels allows for unequivocal relative dating of when the several pulses of quartzose siliciclastic sands and gravels entered the basin [15,33]. The “middle” sandstone member of the Bays Formation in northeastern Tennessee was deposited first (Figure 3), well prior to the eruption of the Deicke tephra [14,15,34,54–56]. The Walker Mountain Sandstone in Virginia and West Virginia was then subsequently deposited nearly coevally with the Deicke K-bentonite [14,15] but well prior to the Millbrig, and finally, the Colvin Mountain Sandstone in Georgia and Alabama was deposited coevally with both the Deicke and the Millbrig [14,15,34]. The three unnamed pebbly sandstones and conglomerates in the Bays Formation near Dalton, Georgia, were deposited after the eruption of the Millbrig tephra [14,34,54–56], but more precise radiometric ages of each of those coarse sands and gravels have not yet been obtained.

We hypothesize that these along-strike variations in the timing of deposition of the mature quartzose sands and gravels relative to the isochronous tephra layers that are now the Deicke and Millbrig K-bentonite beds result from, and can be explained by, a combination of processes driven both by tectonic and climatic events. Deposition of coarser sediments occurring “out of sync” with episodic uplift of tectonic highlands, specifically with deposition lagging uplift, has been documented in the peri-Himalayan region [72–74], as well as during the early stages of the existence of the Blount foredeep in east Tennessee [72,75]. In this scenario, tectonically driven uplift, i.e., folding and thrusting associated with deformation and shortening, was followed by a pulse (or pulses) of coarse molasse sediment moving into and then out across the nearly filled foredeep.

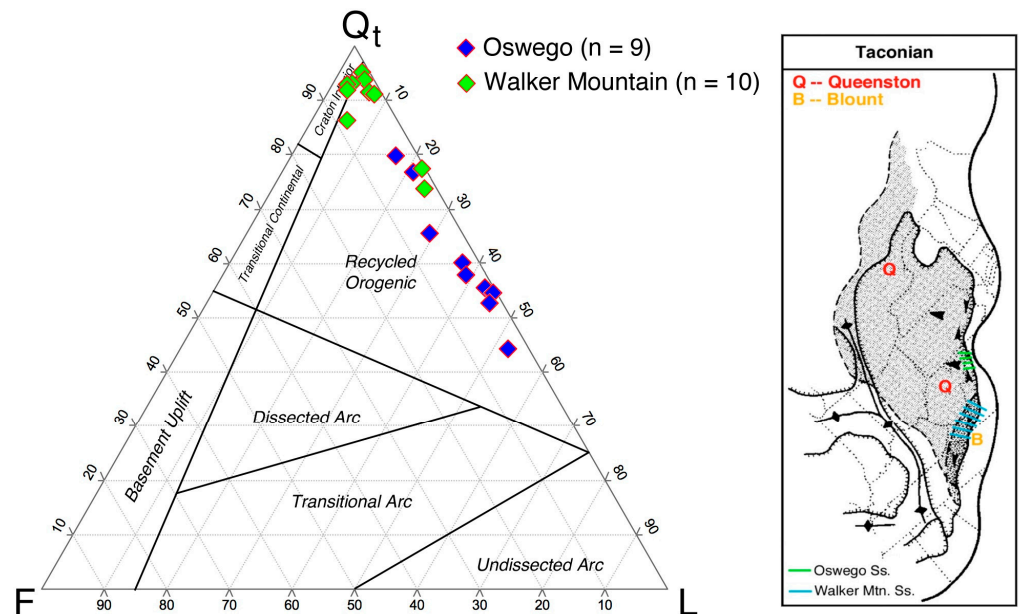


**Figure 10.** Ternary Q/F/L diagram of point-counted thin sections of some of the coarsest Walker Mountain Sandstone samples (from the Trigg, Goodwins Ferry, Gap Mountain, and Mountain Lake Turnoff sections of Haynes [14,34]) with very coarse to conglomeratic Oswego Sandstone samples (from the Brocks Gap, Harshberger Gap, Shenandoah, and Duck Run sections of Diecchio [76]). The Oswego was deposited as part of the younger Queenston molasse during the main Taconian tectophase (inset, right), and it is predominantly a lithic arenite, whereas the Walker Mountain is primarily a quartz arenite to sublithic arenite. The petrographic similarities in lithic fragment compositions, indicated in part by the overlap in the Recycled Orogenic field, suggest that both sandstones likely shared a similar provenance in part (e.g., both sandstones contain vein quartz with vermicular chlorite inclusions), but that the Walker Mountain sands were more extensively washed and winnowed such that they became quartz arenites, quite possibly first-cycle arenites, with most samples plotting in the Craton Interior field. Neither sandstone shows evidence of any component in the sand fraction that was derived from weathering and erosion of a volcanic arc. Ternary diagram modified from Haynes et al. [70]; inset modified from Ettensohn [77].

However, even with active tectonic uplift, the coarse sediments would need a means of presumably fluvial-dominated transport to be moved downslope and into the sediment sink that the Blount foredeep was still serving as, even though it was no longer receiving turbidity currents (as flysch) but was instead a broad area receiving terrestrial muds and the occasional coarse sands and gravels (as molasse). A plausible mechanism that can account for the increased flux of coarser clastics into the nearly filled Blount foredeep regardless of whether—or how much—uplift was occurring in the fold–thrust belt of the Taconic highlands as a result of deformation and shortening is a change to a wetter climate such as has been proposed and debated as a key process in sedimentation patterns of the Himalayan foreland basin and associated sediment sinks including the Indus and Ganges submarine fans [73,74,78–80].

The onset of the modern south Asian monsoonal pattern in the middle Miocene is considered by the above authors to be a driving factor in changes in the Himalayan sedimentary systems. Similarly, we hypothesize that climate change in the Ordovician, specifically the cooling that began prior to the eruption of the Deicke K-bentonite original tephra [81,82], might have been responsible for the mature quartzose sands and gravels that comprise the thin but distinct siliciclastic deposits within the Blount molasse. The cooling around the time of the Deicke likely led to a wetter climate that was presumably accompanied by increased precipitation, and that increase would have facilitated greater and more frequent movement of coarser clastics toward the Blount foredeep. Even though

warming periods [83] episodically punctuated the trend toward a cooling climate at this time, the overall cooler and wetter climate would almost certainly have led to increased rates of erosion via mass wasting and fluvial transport. We suggest that the combination of tectonic and climatic changes at that time is a plausible scenario for the development of the mature to supermature quartz arenites and associated coarser and texturally less mature gravels in the otherwise muddy red bed sequence that characterizes the Blount molasse throughout its extent.

Our detailed stratigraphic work not only demonstrates that delivery of the mature siliciclastic sands and gravels into the Blount foredeep occurred diachronously (oldest in northeast Tennessee, then next oldest in Virginia, and finally youngest in Alabama and Georgia) but also confirms that the Blountian tectophase was a succession of several depositional events rather than one or two events. The earlier pulses of immature to submature coarse sands and gravels that predate the oldest red beds of the molasse and moved into the foredeep as submarine fan lobes and associated turbidity currents (e.g., the conglomerates at Cisco, Georgia, and South Holston Dam, Tennessee [33,56,84]) are populated almost exclusively with clasts of reworked Cambro-Ordovician carbonate rocks rather than with clasts of reworked siliciclastics that would and could have produced the quartz arenites associated with the K-bentonites. Those conglomerates are relatively rare, with by far most of the older strata in the Blount foredeep being turbidites associated with flysch deposition [84–87]. Likewise, younger strata which preserve evidence for a return to shelf carbonate conditions as the regionally widespread “Trenton” transgression occurred subsequent to cessation of molasse deposition are at many sections just a few meters upsection from the quartz arenites and the K-bentonites [54–56,88–90].

#### 4.4. Model for the Formation of Quartz Arenites in the Blount Molasse

##### 4.4.1. Mature Quartz Arenites in Modern Foreland Basins and Implications for Sandstones of the Blount Molasse

The presence of mature to supermature quartz arenites in a foreland basin molasse sequence of otherwise submature to immature finer sands and muds is of interest in constraining temporal and spatial changes in provenance and paleodrainage systems during deposition of the molasse. Plausible Cenozoic analogs for the Ordovician arenites are two mature quartz arenites in the Himalayan foreland basin, the Paleocene to Eocene Bhainskati Formation (Nepal) and the Tura Formation (Bangladesh) [91]. Like the Ordovician arenites that are the focus of our study, orogen-derived detrital zircons have been recovered from those Cenozoic sandstones, and the “puzzling quartzose composition” (as Garzanti [91], p. 16, aptly describes them) of those peri-Himalayan sandstones in an otherwise lithic- and mud-rich sequence of foreland basin deposits is indeed puzzling not only for the Cenozoic arenites but by extension for the Ordovician ones being discussed herein as well. The presence of quartz-rich sands in the Himalayan foredeep has been interpreted [91] as evidence of extensive recycling of older sandstones in tandem with appreciable chemical weathering in humid settings at subequatorial latitudes. The Himalayan foreland comprises a succession of proximal gravels and sands derived from erosion of the rising Himalayan massif that interfinger with finer-grained siliciclastics deposited in the more medial and distal settings of the foreland basin, although coarsening upward in foreland sections largely reflects the motion of the foreland towards the mountain front. Precision dating has shown that the coarse siliciclastic sediments were deposited out of sync with the episodic uplift of the Himalayas [72–74]. This sequence—tectonism in the orogen being followed by a pulse of coarse sediment into the foredeep—has been recognized at other locations as well [72,92], including the Blount foredeep of Tennessee during a time earlier in its existence, before molasse sedimentation began, when it was deepening and receiving sediment via turbidity currents [75]. We suggest that the out-of-sync model of sedimentation developed for other foreland basins, including the Himalayan foredeep, is a viable one for explaining the differences in timing of delivery of the compositionally mature to supermature sands (parts of the Walker Mountain Sandstone of Virginia, and nearly all

of the “middle” sandstone of Tennessee and the Colvin Mountain Sandstone of Georgia and Alabama), as well as the closely associated texturally submature to mature coarse sands and gravels (much of the Walker Mountain Sandstone, and the pebbly sandstones near Dalton, Georgia), into the Blount foredeep during the time that the molasse phase of sedimentation was occurring. Fluvial transport of these sands and gravels likewise may have been enhanced by a changing climate, from a warmer and drier mid-Ordovician climate to a cooler and wetter later Ordovician climate.

Yet another Cenozoic sandstone that we consider highly relevant to this problem and which provides additional insight into how mature quartz sands can be intercalated with less mature muds and sands in a foreland basin is the Oligocene Sirga Formation in the Puncak Jaya region of New Guinea. The Sirga Formation, an extremely mature quartz arenite (>95% quartz) that is 10–100 m thick and is compositionally distinct in an otherwise muddy to calcarenaceous sequence of glauconitic foraminiferal sands and argillaceous packstones, is interpreted as a basal transgressive sand [93], and it overlies a widespread unconformity, a stratigraphic relationship interpreted as evidence of a major but local tectonic event [93,94]. The mature to supermature quartz sands of the Sirga Formation are a very good Cenozoic analog for the mature Ordovician quartz arenites in the Blount molasse, especially the Walker Mountain Sandstone that likewise overlies a regionally significant unconformity in Virginia [14,15,33,54,55], and for the thicker sandstones such as the “middle” sandstone member of the Bays Formation in Tennessee and the Colvin Mountain Sandstone in Alabama and Georgia as well, both of which are sandwiched by red mudrocks and more lithic and finer grained sandstones and siltstones.

We attribute the diachroneity in the age of the Blount quartz arenites from Alabama to Virginia to geographic changes in fluvial networks draining the Taconic highlands, such that over time pulses of gravel and coarse sand were delivered episodically to the coastal region by a depositional complex of braided streams and fan deltas with associated tidal, beach, and fluvial facies, including some with significant eolian influence. Diachroneity might also reflect a climatic gradient that imposes different rates of chemical weathering on different parts of the mountains. We conclude that the depositional system at this time, with its out-of-sync pulses of tectonism and pulses of sediment transport, was governed primarily by tectonic activity rather than eustatic changes, and that a shift to a wetter climate likely contributed to the delivery of gravel and coarse sand to the foredeep as well. Even though there may be an as-yet unrecognized eustatic signal in this Paleozoic stratigraphic interval, it was probably masked or even obliterated in this region by depositional events that were driven by tectonic events in the Taconic highlands, in much the same way that Cenozoic deposition of siliciclastic sediment adjacent to the Himalayan and the New Guinea highlands has been dominated by episodic influx of sands and gravels, including the mature quartz arenites of the Bhainskati Formation (Nepal), the Tura Formation (Bangladesh), and the Sirga Formation (New Guinea) [91,93,94].

For quartz arenites to form, especially first-cycle quartz arenites, a certain combination of environmental factors is needed, because compositionally and texturally mature sand cannot be produced in one cycle under normal conditions associated with weathering, transportation, and deposition [95]. Suttner, Basu, and Mack [96] in fact concluded that most quartz arenites in the rock record are of multicycle origin because there is a low probability that such conditions would occur in the past with any regularity. Reworking of older proximal foreland sediments following erosional unloading of the orogenic load has been invoked as the trigger for the deposition of compositionally mature sediments in the distal foreland of the Rockies [97]. A humid climate is considered to be a requirement that must be met if first-cycle quartz arenites are to form [98,99], because of the importance of chemical weathering over physical weathering at all stages, beginning at the source and extending throughout the duration of grain transport and probably deposition as well so as to ensure adequate time for the complete destruction of less resistant grains via decomposition and disintegration [100].

#### 4.4.2. Climate Conditions Required for Generation of Mature Quartz Arenites in the Ordovician of the Southern Appalachians

Various studies have linked the later Ordovician transition to the end-Ordovician Hirnantian glaciation with an increase in chemical weathering [101,102]). Recent paleotemperature estimates based on conodont apatite suggest that warming had already occurred across the interval of time when the explosive volcanism responsible for the Deicke and Millbrig K-bentonites occurred [82,83,103,104]. Furthermore, Nd isotopic studies of conodont apatite support the interpretation that this was a time characterized by increased rates of weathering [105], and Swanson-Hysell and Macdonald [106] suggest that by 465 Ma, the Appalachian margin of Laurentia was in a warm, humid, tropical setting (between 0° and 10° S latitude at that time), consistent with climate modeling results [107–109]. Thus, our hypothesis that sediments eroded from the Taconic highlands could be weathered relatively rapidly into mature quartz arenites is bolstered by these constraints on climate, even if the quartzose sands and gravels described herein are all first-cycle arenites. U-Pb geochronology of detrital zircons from mature Cambro-Ordovician quartz sandstones of northern Gondwana [98] indicates that those Lower Paleozoic units are first-cycle arenites [110,111], whereas South America's Orinoco River drainage basin, which at 8° N of the Equator exists in a tropical humid climate, is a modern analog for how and where first-cycle quartz arenites develop [112]. Therefore, we conclude that the quartz arenites of the Ordovician molasse in the southern Appalachians were very likely generated under similar conditions, i.e., intense chemical weathering of terrigenous sediments in the tropical environments along the Laurentian margin in the Late Ordovician, with intermittent and alternating periods of transport and storage as alluvium in, along, across, and ultimately through fluvial flood plains and low-elevation coastal plains similar to those in the Orinoco basin today.

#### 4.5. Evaluation of Tectonostratigraphic “Retroarc Basin” Model

Mapping and analysis of metasediments in the Wedowee–Emuckfaw–Dahlonega (WED) Basin of the Blue Ridge and Piedmont provinces in the southern Appalachians have led to the development of an alternate hypothesis for the tectonic setting of Laurentia's southeastern margin during the later Ordovician. This alternate “Sea of Japan” model proposes that an Ordovician back-arc basin developed along the Laurentian margin, with the development of the Blount foreland basin in particular being attributed to the inversion of Neoproterozoic rift-related faults; furthermore, the Blount basin at that time (i.e., ~465 Ma) is hypothesized to have been in a retroarc position, on the Laurentian side of the WED Basin [24–26,113,114].

This alternate model requires that a switch in subduction polarity along the Laurentian margin occurred, from an east-dipping system farther north to a west-dipping system in this area, and the model also does not recognize an accretionary prism in the southern Appalachians at this time. In fact, those authors invoked the hypothesized switch of polarity to account for the apparent absence of an accretionary wedge, whereas the older (east-dipping) model includes an accretionary prism [32]. Furthermore, in this alternate retroarc model, the K-bentonites in the Ordovician sedimentary sequences found in today's Valley and Ridge are hypothesized to have been sourced from eruptions associated with extensionally-thinned Laurentian continental crust (Figure 2D), a scenario that is suggested as a means of accounting for the requirement that a source of felsic magma be present to source the immense explosive eruptions that produced the tephra that are now the Deicke and Millbrig K-bentonites.

However, because silica content correlates positively with crustal thickness, and rhyolitic calderas appear only on crust that is >25 km thick (Hughes and Mahood [115]), the hypothesis that the volcanoes which sourced the tephra that are now the Deicke and Millbrig K-bentonites (as well as the many other K-bentonites in the Ordovician of this region [14]) were developed on extensionally thinned Laurentian crust poses a problem for the retroarc model, because it is incompatible with the requirement that the

most voluminous and regionally widespread K-bentonites were necessarily sourced from huge caldera-forming eruptions, the only eruptions known to be of sufficient magnitude to account for erupted tephra that have the extent and composition of the Deicke and Millbrig K-bentonites [14–18].

Furthermore, the retroarc model does not account for the thin but widespread quartz arenites of the Blount molasse that are the focus herein. There is a near total lack of Paleozoic zircons within the Taconic clastic wedge [116,117], and the detrital zircons we have analyzed imply that the older recycled zircons derive from a source terrain that was unroofed during the Taconic orogeny. The likeliest source is in fact the older foreland sedimentary sequences that were upturned and deformed along the active Laurentian margin in the tectonic highlands, with some of the zircons having weathered out of those older sediments and then being transported subsequently with the sands that became the Blount molasse quartz arenites. Previous researchers speculated that the lack of older Paleozoic sediments in the Taconic foredeep could be attributed to sequestering behind an accretionary prism (Figure 2B) that developed and evolved in the later Ordovician [3]. This is consistent with modern foreland basins because many of them are separated from their associated magmatic arc(s) by a forearc basin and forearc ridge system that is typically composed of an accretionary prism [118,119]. Until erosion opens one or more transport pathways across and through this accretionary mass, little if any arc-derived sediments will accumulate in the foredeep [69].

The WED Basin retroarc basin model lacks such an accretionary wedge that would have been facing the continental margin. The tectonic constraints of the retroarc basin model would have the accretionary prism situated on the outer margin of the retroarc complex, and thus the accretionary wedge would likely have scraped off trench sediments and perhaps a minor component of pelagic sediments from the seafloor, e.g., radiolarian cherts and associated oozes and red clay deep-sea oceanic sediments of the Iapetus Ocean, rather than Precambrian to Early Ordovician continental margin sediments that are the most probable source(s) of the observed detrital zircon age spectra.

The presence of Ordovician-age rims in detrital zircons from the Colvin Mountain Sandstone in Georgia and Alabama and the confirmation (based on apatite phenocryst geochemistry) that the Deicke and Millbrig K-bentonites are unequivocally present in the Colvin Mountain Sandstone are critical findings. They confirm that the quartzose sands at those exposures were being deposited after one or both of those two K-bentonite beds had been erupted, and they also suggest that the mature quartz sands must have been deposited downwind some distance from the eruptive centers, assuming that some of the detrital zircons, i.e., those without inherited cores, were in fact deposited as phenocrysts in airfall tephra that then co-mingled with the quartzose sands.

Finally, the presence of older, rounded inherited cores in some of the zircons that have a Taconic age component in their rims is most readily explained by subduction of older sedimentary sequences that included detrital zircons derived from weathering and erosion of older rock of Grenville/Keweenawan, Granite–Rhyolite age, etc., with the rounding of those zircons that are now seen as inherited cores having taken place during one or more prior erosional cycles [37]. As subduction of these older strata occurred during the Taconic Orogeny, some of the older zircons would likely have been assimilated intact into the rising magma, a process that has been documented in modern subduction settings [48,49]. Such a process is not supported in the retroarc model; therefore, we conclude that a key subordinate part of that model, which is that the Blount foredeep developed as a retroarc basin along the southern margin of Laurentia as part of a larger back-arc system, is likewise untenable.

#### 4.6. Evaluation of “The Australian Margin Tectonic Model” as a Potential Analog

The island of New Guinea is the leading edge of the Australian plate along its active convergent northeastern margin. This northern edge of the Australian plate and its various arcs and microcontinents and terranes makes a good analog for the Taconic highland massif of the later Ordovician. Collision with an island arc in the early Tertiary produced mélanges

and obducted ophiolites between the Australian continent and the accreted arc in New Guinea. Accretion of the arc caused a subduction polarity reversal, forming the current-day southwest-dipping subduction zone north of New Guinea [93,118,120–124]. This island arc–continent collision is an excellent model for the Ordovician Taconic orogeny, as it is widely agreed that the likely cause of the Taconic orogeny was an island arc colliding with the Laurentian margin. The northern edge of the Australian plate has been deformed by this ongoing collision into the fold-and-thrust belt of the New Guinea highlands, with an associated foreland basin developed on downwarped Australian continental crust that is cratonward of the active margin, i.e., the area now flooded by the eastern Arafura Sea, the Torres Strait, the Gulf of Carpentaria, and the Gulf of Papua. The similarity between this region and the Appalachians has been noted previously, in that New Guinea and the central and southern Appalachians occupy approximately the same size area, both have similar tectonic belts, and both have a comparable geochronological pattern [125].

A sedimentary link between continental Australia and nearby areas including New Guinea and the Banda Arc has also been documented. A provenance study of detrital zircons in sandstones demonstrated that certain quartzose sandstones from the Bird's Head region of New Guinea were derived from the Australian craton [126]. The strata along the Mapenduma anticline in the New Guinea highlands block include reworked Precambrian Australian craton sediments [94,121–127], and Precambrian zircons also occur in Permian metasedimentary rocks from the Kubor and Bena Bena blocks of the Central Highlands, the Late Miocene Porgera intrusive complex in the New Guinea fold belt, and Plio-Pleistocene sediments of the Trobriand Basin of the Woodlark Rift [128,129]. Cretaceous sandstones in the Banda Arc likewise were derived in part from the Bird's Head and cratonic Australia [130]. In addition, the foreland basin adjacent to the New Guinea highlands also includes clastic sediments that were derived primarily from older shelf strata uplifted in the mountains [118].

#### 4.7. Evaluation of the “The Sumatra/Toba Tectonic Model” as a Potential Analog

Smith et al. [131] and Chesner [132] reported petrologic details of the 75 ka Toba Tuffs of Sumatra, one of which is the presence of abundant ferroan-rich phenocrystic biotite. Of particular note is that the major element abundances in the Older and Middle Toba Tuffs are notable for being similar in composition to the abundances of the same major elements in the abundant biotite that is characteristic of the lower tuffaceous zone of the Millbrig K-bentonite in our study region [14,133,134]. This compositional similarity led us to hypothesize that the Ordovician K-bentonites are almost certainly the product of immense explosive, caldera-forming volcanic eruptions [134], and because such eruptions are invariably associated with continental crust [135,136], e.g., the Toba volcanic system, which developed above Permian to Cretaceous granites of the Sumatran basement [118], a continental crust basement is considered to be an unassailable requirement for the Ordovician magmatic arc as well.

The tectonic setting of modern Sumatra is not a simple analog for the Ordovician foreland basin of Laurentia's eastern margin, but with a little imagination, we can visualize that if the island of Sumatra—with the Toba caldera—were juxtaposed with the island of New Guinea, a better overall paleogeographic arrangement would then exist. With this hypothetical juxtaposition of Sumatra, we would have (1) the modern Australian craton as the analog to the Ordovician Laurentian craton; (2) New Guinea combined with Sumatra and the Toba caldera as the analog to the Ordovician Taconic highlands and associated volcanic centers from which the major Ordovician tephtras were erupted; (3) deformation and erosion of older sedimentary sequences along the southern margin of New Guinea as the source of the muds, sands, and gravels that are analogous to the Ordovician molasse sediments, and which all lack appreciable sediment derived from the volcanic arc; and (4) the Timor Sea, Arafura Sea, and Gulf of Carpentaria as the analog to the Taconic foreland basin, with both foredeeps developed on downwarped continental crust. Thus, we hypothesize that during the later Ordovician, a Toba-style eruption (in terms of

magnitude and composition) was responsible for producing the biotite-rich tephra that is now the Millbrig K-bentonite. This would also require that, prior to eruption, the magma had interacted with continental crust in order to generate the ferroan-rich biotite found in the Millbrig, biotite that is remarkably close in composition to the abundant ferroan-rich phenocrystic biotite of the Older and Middle Toba Tuffs, generated from magma that interacted with the granitic basement of Sumatra.

## 5. Conclusions

BSE images and U-Pb geochronology of several detrital zircons from Ordovician sandstones in the southern Appalachians show that some of the zircons have old cores and Taconic-aged rims. We attribute this difference in ages to magmatic activity along the Taconic convergent margin, and specifically to a subduction zone in which incomplete melting of continental crust allowed for the incorporation of Grenville-aged zircons into the ascending melt. This incorporation of continental sediments was a key component for the generation of felsic melts, a process that was crucial to the development of massive, caldera-forming explosive volcanic eruptions that generated the tephtras now preserved as the voluminous and widespread Deicke and Millbrig K-bentonites, because explosive eruptions of that magnitude are sourced by felsic magmas with a relatively high silica content. In the northern Appalachians, high silica magmatism during collision has likewise been noted [137]. The northern Australian margin and the Toba caldera on Sumatra, or some combination thereof, collectively provide modern analogs that are suitable models for the Laurentian margin during the later Ordovician. These would be suitable for explaining the required felsic magma source capable of generating caldera-forming eruptions. The Sirga Formation of New Guinea [93] is a suitable proxy for the mature pebbly quartz arenites of the Colvin Mountain Sandstone, Walker Mountain Sandstone, and other similar units in the otherwise muddy molasse red bed sequence of the Bays, Moccasin, and Greensport formations from Virginia to Alabama [14].

These Ordovician quartz arenites and their detrital zircons clearly have a multicycle sediment component. Similar to what is seen today around the Timor and Arafura seas and the Gulf of Carpentaria, older sedimentary sequences would have been uplifted in the Taconic highlands and then deformed, weathered, and ultimately eroded, with the zircons therein eventually being deposited within the molasse sequence during the later stages of filling of the Blount foreland basin. Petrographic evidence supports an interpretation that there was an appreciable first-cycle quartz arenite component for some of these Ordovician sands and gravels. The maturity of the Ordovician quartz arenites likely resulted from the intensification of chemical weathering acting on the recycled sediments coming off an exposed forearc ridge and/or an accretionary prism that was part of the Taconic highlands massif. This increased rate of chemical weathering would have resulted in the destruction of nearly all feldspars and other less durable lithic fragments. As the sands and gravels were being transported to the foredeep by rivers, it is likely that the process was interrupted episodically by long intervals of storage in the flood plains that were part of a larger coastal plain environment, similar to how first-cycle quartz arenites have formed in the Orinoco River drainage basin of South America [99].

Based on stratigraphic relationships with two isochrons, the altered layers of airfall tephra that are now confirmed as the Deicke and Millbrig K-bentonite beds on the basis of their apatite phenocryst geochemistry, we reaffirm that these coarse but compositionally mature sands and gravels entered the basin first in the area of east Tennessee (the “middle” sandstone member of the Bays Formation), then in western and southwestern Virginia (the Walker Mountain Sandstone), and then finally in Georgia and Alabama (the Colvin Mountain Sandstone). Both the “middle” sandstone and the Walker Mountain Sandstone are older than the Deicke K-bentonite, and then subsequently sands of similar composition were delivered to the foredeep as the Colvin Mountain Sandstone, which either immediately overlies the Deicke K-bentonite, or immediately overlies the Millbrig K-bentonite, or completely encloses both the Deicke and Millbrig K-bentonite beds. The

final pulse may be represented by the very coarse sands and gravels in north Georgia that occur about 2–3 m above the Millbrig K-bentonite, but precise radiometric ages of detrital zircons from that conglomerate have not yet been obtained. The U-Pb ages acquired from detrital zircons in these sandstones point to most of those zircons being sourced from the Laurentian craton, with ~96.5% of all ages being older than the later Ordovician.

**Supplementary Materials:** The following supporting information can be downloaded at: <https://www.mdpi.com/article/10.3390/min13060807/s1>, Table S1: U-Pb age data for the sandstones at Horseleg Mountain, Dodson Mountain, Crockett Cove, Gap Mountain, and secondary standards Temore2 and Plesovice. U-Pb age data for the sandstones at Alexander Gap, Dirtseller Mountain, and Hanging Rock can be accessed from [49]. Included are the secondary standards; Table S2: Elemental composition of magmatic apatites used for geochemical fingerprinting. Included are the secondary standards.

**Author Contributions:** Conceptualization, A.D.H. and J.T.H.; methodology, A.D.H. and J.T.H.; apatite phenocryst analyses and data validation, R.R.; magmatic zircon phenocryst analyses and data validation, A.D.H.; detrital zircon phenocryst analyses and data validation, J.T.H. and A.D.H.; sedimentological analysis and interpretation, J.T.H. and K.E.G.; sandstone petrography, J.T.H. and K.E.G.; data curation, A.D.H.; writing—original draft preparation, A.D.H. and J.T.H.; writing—review and editing, A.D.H., J.T.H., P.D.C., R.R. and K.E.G.; supervision of research, A.D.H. and J.T.H.; funding acquisition, A.D.H. All authors have read and agreed to the published version of the manuscript.

**Funding:** This research was funded by the US National Science Foundation (grant number EAR-1324954). The APC was funded by the journal. RMR acknowledges support from the Marathon Oil Corporation and the LSU Department of Geology & Geophysics in the form of the Geoscience Diversity Enrichment Program (GeoDE). JTH acknowledges the Tickle Scholarship program at James Madison University for supporting JMU geology student Ryan Cleveland in 2015.

**Data Availability Statement:** Not available.

**Acknowledgments:** ADH thanks Jürgen Konzett (University of Innsbruck) for CL imaging of zircons. The authors thank SelFrag (especially Steve Gennatos, Daniel Parvaz, and Alexander Weh) for allowing the use of a demo lab of SelFrag for this study. JTH thanks Lee Suttner (Indiana University) for his inspired teaching about sandstones during field camp at Cardwell in 1980, Paul Potter (University of Cincinnati) for sparking a deep interest in sandstones and for all that he taught about sandstone petrology, Rick Diecchio (George Mason University) for advice and countless helpful conversations over many years about these strata, Tim Rose (Smithsonian Institution) for his assistance with many mineral analyses over the years, and especially Warren Huff (University of Cincinnati) for his role as a mentor and for all the field work and discussions about Ordovician K-bentonites over the decades.

**Conflicts of Interest:** The authors declare no conflict of interest.

## References

1. Rodgers, J. The taconic orogeny. *Geol. Soc. Am. Bull.* **1971**, *82*, 1141–1178. [[CrossRef](#)]
2. Coler, D.G.; Wortman, G.L.; Samson, S.D.; Hibbard, J.P.; Stern, R. U-Pb Geochronologic, Nd Isotopic, and Geochemical Evidence for the Correlation of the Chopawamsic and Milton Terranes, Piedmont Zone, Southern Appalachian Orogen. *J. Geol.* **2000**, *108*, 363–380. [[CrossRef](#)]
3. Eriksson, K.A.; Campbell, I.H.; Palin, J.M.; Allen, C.M.; Bock, B. Evidence for Multiple Recycling in Neoproterozoic through Pennsylvanian Sedimentary Rocks of the Central Appalachian Basin. *J. Geol.* **2004**, *112*, 261–276. [[CrossRef](#)]
4. Chapple, W.M. Taconic orogeny: Abortive subduction of the North American continental plate? *Geol. Soc. Am. Abstr. Programs* **1973**, *5*, 573.
5. Robinson, P.; Hall, L.M. Tectonic synthesis of southern New England. *Int. Geol. Correl. Proj. Proc. Proj.* **1980**, *27*, 73–82.
6. Rowley, D.B.; Kidd, W.S.F. Stratigraphic relationships and detrital composition of the medial Ordovician flysch of western New England: Implications for the tectonic evolution of the Taconic orogeny. *J. Geol.* **1981**, *89*, 199–218. [[CrossRef](#)]
7. Stanley, R.S.; Ratcliffe, N.M. Tectonic synthesis of the Taconian orogeny in western New England. *Geol. Soc. Am. Bull.* **1985**, *96*, 1227–1250. [[CrossRef](#)]
8. Karabinos, P.; Samson, S.D.; Hepburn, J.C.; Stoll, H.M. Taconian orogeny in the New England Appalachians: Collision between Laurentia and the Shelburne Falls arc. *Geology* **1998**, *26*, 215–218. [[CrossRef](#)]

9. Waldron, J.W.F.; van Staal, C.R. Taconian orogeny and the accretion of the Dashwoods block: A peri-Laurentian microcontinent in the Iapetus Ocean. *Geology* **2001**, *29*, 811–814. [[CrossRef](#)]
10. van Staal, C.R.; Whalen, J.B.; McNicoll, V.J.; Pehrsson, S.; Lissenberg, C.J.; Zagorevski, A.; Van Breemen, O.; Jenner, G.A. The Notre Dame arc and the Taconic orogeny in Newfoundland. *Geol. Soc. Am. Mem.* **2007**, *200*, 511–552.
11. Zagorevski, A.; Rogers, N.; Van Staal, C.R.; McNicoll, V.; Lissenberg, C.J.; Valverde-Vaquero, P. Lower to Middle Ordovician evolution of peri-Laurentian arc and backarc complexes in Iapetus: Constraints from the Annieopsquotch accretionary tract, central Newfoundland. *Geol. Soc. Am. Bull.* **2006**, *118*, 324–342. [[CrossRef](#)]
12. Herrmann, A.D.; Haynes, J.T.; Robinet, R.M.; Emerson, N.R. Machine Learning Applied to K-Bentonite Geochemistry for Identification and Correlation: The Ordovician Hagan K-Bentonite Complex Case Study. *Geosciences* **2021**, *11*, 380. [[CrossRef](#)]
13. Guerrero, J.C. Reinterpreting the Tectonic Model of the Southern Part of the Taconic Orogeny through a Provenance Study of Late Ordovician Sandstone. Master's Thesis, Louisiana State University and Agricultural and Mechanical College, Baton Rouge, LA, USA, 2019. [[CrossRef](#)]
14. Haynes, J.T. *The Ordovician Deicke and Millbrig K-Bentonite Beds of the Cincinnati Arch and the Southern Valley and Ridge Province*; Geological Society of America Special Papers; Geological Society of America: Boulder, CO, USA, 1994; Volume 290, pp. 1–80.
15. Haynes, J.T.; Goggin, K.E. *Stratigraphic Relations of Quartz Arenites and K-Bentonites in the Ordovician Blount Molasse, Alabama to Virginia, Southern Appalachians, USA*; Gutiérrez-Marco, J.C., Ed.; Instituto Geológico y Minero de España: Madrid, Spain; Ordovician of the World: Madrid, Spain, 2011; pp. 221–228.
16. Huff, W.D. Ordovician K-bentonites: Issues in interpreting and correlating ancient tephros. *Quat. Int.* **2008**, *178*, 276–287. [[CrossRef](#)]
17. Huff, W.D.; Bergström, S.M.; Kolata, D.R. Gigantic Ordovician volcanic ash fall in North America and Europe: Biological, tectonomagmatic, and event-stratigraphic significance. *Geology* **1992**, *20*, 875–878. [[CrossRef](#)]
18. Huff, W.D.; Bergström, S.M.; Kolata, D.R. *Ordovician Explosive Volcanism*; Geological Society of America Special Papers; Geological Society of America: Boulder, CO, USA, 2010; Volume 466, pp. 13–28.
19. Tucker, R.D.; McKerrow, W.S. Early Paleozoic chronology: A review in light of new U–Pb zircon ages from Newfoundland and Britain. *Can. J. Earth Sci.* **1995**, *32*, 368–379. [[CrossRef](#)]
20. Sell, B.; Ainsaar, L.; Leslie, S. Precise timing of the Late Ordovician (Sandbian) super-eruptions and associated environmental, biological, and climatological events. *J. Geol. Soc.* **2013**, *170*, 711–714. [[CrossRef](#)]
21. Huff, W.D.; Kolata, D.R. Correlation of the Ordovician Deicke and Millbrig K-Bentonites between the Mississippi Valley and the Southern Appalachians (1). *AAPG Bull.* **1990**, *74*, 1736–1747.
22. Kolata, D.R.; Huff, W.D.; Bergstrom, S.M. *Ordovician K-Bentonites of Eastern North America*; Geological Society of America: Boulder, CO, USA, 1996; Volume 313.
23. Kolata, D.R.; Huff, W.D.; Bergstrom, S.M. Nature and regional significance of unconformities associated with the Middle Ordovician Hagan K-bentonite complex in the North American midcontinent. *Geol. Soc. Am. Bull.* **1998**, *110*, 723–739. [[CrossRef](#)]
24. Barineau, C.; Tull, J.F.; Holm-Denoma, C.S. A Laurentian margin back-arc: The Ordovician Wedowee-Emuckfaw-Dahlongega basin. *Geol. Soc. Am. Field Guid.* **2015**, *39*, 21–78.
25. Barineau, C.I.; Sagul, D.A.; Mueller, P.A. Ordovician–Silurian back-arc silicic magmatism in the southernmost Appalachians. *GSA Bull.* **2022**, *134*, 2321–2334. [[CrossRef](#)]
26. Tull, J.; Holm-Denoma, C.S.; Barineau, C.I. Early to Middle Ordovician back-arc basin in the southern Appalachian Blue Ridge: Characteristics, extent, and tectonic significance. *Geol. Soc. Am. Bull.* **2014**, *126*, 990–1015. [[CrossRef](#)]
27. Tull, J.F.; Mueller, P.A.; Farris, D.W.; Davis, B.L. Taconic suprasubduction zone magmatism in southern Laurentia: Evidence from the Dadeville Complex. *Geol. Soc. Am. Bull.* **2018**, *130*, 1339–1354. [[CrossRef](#)]
28. Farris, D.W.; Tull, J.; Mueller, P.; Davis, B. Is the Dadeville Complex part of the “missing” Southern Appalachian Taconic Arc? *Ga. Geol. Soc. Guideb.* **2017**, *36*, 41–56.
29. Shanmugam, G.; Lash, G.G. Analogous tectonic evolution of the Ordovician foredeeps, southern and central Appalachians. *Geology* **1982**, *10*, 562–566. [[CrossRef](#)]
30. Brookfield, M.E.; Brett, C.E. Paleoenvironments of the mid-Ordovician (Upper Caradocian) Trenton limestones of southern Ontario, Canada: Storm sedimentation on a shoal-basin shelf model. *Sediment. Geol.* **1988**, *57*, 75–105. [[CrossRef](#)]
31. Knight, I.; James, N.P.; Lane, T.E. The Ordovician St. George Unconformity, northern Appalachians: The relationship of plate convergence at the St. Lawrence Promontory to the Sauk/Tippecanoe sequence boundary. *Geol. Soc. Am. Bull.* **1991**, *103*, 1200–1225. [[CrossRef](#)]
32. Mussman, W.J.; Read, J.F. Sedimentology and development of a passive- to convergent-margin unconformity: Middle Ordovician Knox unconformity, Virginia Appalachians. *Geol. Soc. Am. Bull.* **1986**, *97*, 282–295. [[CrossRef](#)]
33. Herrmann, A.; Haynes, J.T. Ordovician of the Southern Appalachians, USA Pre-Symposium Field Trip. *Stratigraphy* **2015**, *12*, 203–251.
34. Haynes, J.T. *Reinterpretation of Rocklandian (Upper Ordovician) K-Bentonite Stratigraphy in Southwest Virginia, Southeast West Virginia, and Northeast Tennessee, with a Discussion of the Conglomeratic Sandstones in the Bays and Moccasin Formations*; Commonwealth of Virginia, Department of Mines, Minerals, and Energy, Division of Mineral Resources: Charlottesville, VA, USA, 1992; Volume 126, pp. 1–58.

35. Cantine, M.D.; Setera, J.B.; Vantongerren, J.A.; Mwinde, C.; Bergmann, K.D. Grain size and transport biases in an Ediacaran detrital zircon record. *J. Sediment. Res.* **2021**, *91*, 913–928. [[CrossRef](#)]
36. Sell, B.K.; Samson, S.D.; Mitchell, C.E.; McLaughlin, P.I.; Koenig, A.E.; Leslie, S.A. Stratigraphic correlations using trace elements in apatite from Late Ordovician (Sandbian-Katian) K-bentonites of eastern North America. *Geol. Soc. Am. Bull.* **2015**, *127*, 1259–1274. [[CrossRef](#)]
37. Herrmann, A.D.; Haynes, J.T.; Robinet, R.M.; Konzett, J.; Emerson, N.R. Insights into the tectonostratigraphic setting of the Southern Appalachians during the Blountian tectophase from an integrated geochemical analysis of magmatic phenocrysts in the Ordovician Deicke K-bentonite. *Lithos* **2021**, *398*, 106301. [[CrossRef](#)]
38. Hellstrom, J.; Paton, C.; Woodhead, J.; Hergt, J. *Iolite: Software for Spatially Resolved LA-(quad and MC) ICPMS Analysis*; Mineralogical Association of Canada Short Course Series; Mineralogical Association of Canada: Québec, QC, Canada, 2008; Volume 40, pp. 343–348.
39. Wiedenbeck, M.; Alle, P.; Corfu, F.; Griffin, W.L.; Meier, M.; Oberli, F.v.; Quadt, A.v.; Roddick, J.; Spiegel, W. Three natural zircon standards for U-Th-Pb, Lu-Hf, trace element and REE analyses. *Geostand. Newsl.* **1995**, *19*, 1–23. [[CrossRef](#)]
40. Horstwood, M.S.; Košler, J.; Gehrels, G.; Jackson, S.E.; McLean, N.M.; Paton, C.; Pearson, N.J.; Sircombe, K.; Sylvester, P.; Vermeesch, P. Community-derived standards for LA-ICP-MS U-(Th)-Pb geochronology—Uncertainty propagation, age interpretation and data reporting. *Geostand. Geoanal. Res.* **2016**, *40*, 311–332. [[CrossRef](#)]
41. Black, L.P.; Kamo, S.L.; Allen, C.M.; Aleinikoff, J.N.; Davis, D.W.; Korsch, R.J.; Foudoulis, C. TEMORA 1: A new zircon standard for Phanerozoic U–Pb geochronology. *Chem. Geol.* **2003**, *200*, 155–170. [[CrossRef](#)]
42. Sláma, J.; Košler, J.; Condon, D.J.; Crowley, J.L.; Gerdes, A.; Hanchar, J.M.; Horstwood, M.S.; Morris, G.A.; Nasdala, L.; Norberg, N. Plešovice zircon—A new natural reference material for U–Pb and Hf isotopic microanalysis. *Chem. Geol.* **2008**, *249*, 1–35. [[CrossRef](#)]
43. Petrus, J.A.; Kamber, B.S. VizualAge: A Novel Approach to Laser Ablation ICP-MS U-Pb Geochronology Data Reduction. *Geostand. Geoanal. Res.* **2012**, *36*, 247–270. [[CrossRef](#)]
44. Paton, C.; Hellstrom, J.; Paul, B.; Woodhead, J.; Hergt, J. Iolite: Freeware for the visualisation and processing of mass spectrometric data. *J. Anal. At. Spectrom.* **2011**, *26*, 2508–2518. [[CrossRef](#)]
45. Carey, A.; Samson, S.D.; Sell, B. Utility and limitations of apatite phenocryst chemistry for continent-scale correlation of Ordovician K-bentonites. *J. Geol.* **2009**, *117*, 1–14. [[CrossRef](#)]
46. Tapster, S.; Roberts, N.M.W.; Petterson, M.G.; Saunders, A.D.; Naden, J. From continent to intra-oceanic arc: Zircon xenocrysts record the crustal evolution of the Solomon island arc. *Geology* **2014**, *42*, 1087–1090. [[CrossRef](#)]
47. Kröner, A. The role of geochronology in understanding continental evolution. *Geol. Soc. Lond. Spec. Publ.* **2010**, *338*, 179–196. [[CrossRef](#)]
48. Shao, W.-Y.; Chung, S.-L.; Chen, W.-S.; Lee, H.-Y.; Xie, L.-W. Old continental zircons from a young oceanic arc, eastern Taiwan: Implications for Luzon subduction initiation and Asian accretionary orogeny. *Geology* **2015**, *43*, 479–482. [[CrossRef](#)]
49. Smyth, H.R.; Hamilton, P.J.; Hall, R.; Kinny, P.D. The deep crust beneath island arcs: Inherited zircons reveal a Gondwana continental fragment beneath East Java, Indonesia. *Earth Planet. Sci. Lett.* **2007**, *258*, 269–282. [[CrossRef](#)]
50. Aitchison, J.C.; Cluzel, D.; Ireland, T.R.; Zhou, R.; Lian, D.; Patias, D.; Yan, Z.; Yang, J. Solid-phase transfer into the forearc mantle wedge: Rutile and zircon xenocrysts fingerprint subducting sources. *Earth Planet. Sci. Lett.* **2022**, *577*, 117251. [[CrossRef](#)]
51. Samson, S.D.; Kyle, P.R.; Alexander, J.E.C. Correlation of North American Ordovician bentonites by using apatite chemistry. *Geology* **1988**, *16*, 444. [[CrossRef](#)]
52. Van der Pluijm, B.A.; Marshak, S. *Earth Structure*; W.W. Norton: New York, NY, USA, 2004.
53. Ettensohn, F.R.; Lierman, R.T. Large-Scale Tectonic Controls on the Origin of Paleozoic Dark-Shale Source-Rock Basins: Examples from the Appalachian Foreland Basin, Eastern United States. In *Tectonics and Sedimentation Implications for Petroleum Systems*; American Association of Petroleum Geologists: Tulsa, OK, USA, 2012.
54. Haynes, J.T.; Goggin, K.E. Field guide to the Ordovician Walker Mountain Sandstone Member: Proposed type section and other exposures. *Va. Miner.* **1993**, *39*, 25–37.
55. Haynes, J.T.; Goggin, K.E. K-bentonites, conglomerates, and unconformities in the Ordovician of southwestern Virginia. In *Field Guides to Southern Appalachian Structure, Stratigraphy, and Engineering Geology: Virginia Tech Department of Geological Sciences Guidebook*; Virginia Polytechnic Institute and State University: Blacksburg, VA, USA, 1994; pp. 65–93.
56. Hergenroder, J.D. The Bays Formation (Middle Ordovician) and Related Rocks of the Southern Appalachians. Ph.D. Dissertation, Virginia Polytechnic Institute and State University, Blacksburg, VA, USA, 1966.
57. Retallack, G.J. Scoyenia burrows from Ordovician palaeosols of the Juniata Formation in Pennsylvania. *Palaeontology* **2001**, *44*, 209–235. [[CrossRef](#)]
58. Díez-Canseco, D.; Buatois, L.A.; Mángano, M.G.; Díaz-Molina, M.; Benito, M.I. Ichnofauna from coastal meandering channel systems (Upper Cretaceous Tresp Formation, South-Central Pyrenees, Spain): Delineating the fluvial-tidal transition. *J. Paleontol.* **2016**, *90*, 250–268. [[CrossRef](#)]
59. Toom, U.; Vinn, O.; Hints, O. Ordovician and Silurian ichnofossils from carbonate facies in Estonia: A collection-based review. *Palaeoworld* **2019**, *28*, 123–144. [[CrossRef](#)]
60. Davies, N.S.; Gibling, M.R.; Rygel, M.C. Alluvial facies evolution during the Palaeozoic greening of the continents: Case studies, conceptual models and modern analogues. *Sedimentology* **2011**, *58*, 220–258. [[CrossRef](#)]

61. Prave, A.R. Depositional and sequence stratigraphic framework of the Lower Cambrian Zabriskie Quartzite: Implications for regional correlations and the Early Cambrian paleogeography of the Death Valley region of California and Nevada. *Geol. Soc. Am. Bull.* **1992**, *104*, 505–515. [\[CrossRef\]](#)
62. McBride, E.F. Petrology of the Eureka Quartzite (Middle and Late Ordovician), Utah and Nevada, U.S.A. *Rocky Mt. Geol.* **2012**, *47*, 81–111. [\[CrossRef\]](#)
63. Yang, B.; Gingras, M.K.; Pemberton, S.G.; Dalrymple, R.W. Wave-generated tidal bundles as an indicator of wave-dominated tidal flats. *Geology* **2008**, *36*, 39–42. [\[CrossRef\]](#)
64. Tape, C.H.; Cowan, C.A.; Runkel, A.C. Tidal-Bundle Sequences in the Jordan Sandstone (Upper Cambrian), Southeastern Minnesota, U.S.A.: Evidence for Tides along Inboard Shorelines of the Sauk Epicontinental Sea. *J. Sediment. Res.* **2003**, *73*, 354–366. [\[CrossRef\]](#)
65. Mack, G.H. Provenance of the Middle Ordovician Blount clastic wedge, Georgia and Tennessee. *Geology* **1985**, *13*, 299–302. [\[CrossRef\]](#)
66. Belkin, H.E.; Repetski, J.E.; Dulong, F.T.; Hickling, N.L. Lithologies, ages, and provenance of clasts in the Ordovician Fincastle Conglomerate, Botetourt County, Virginia, USA. *Stratigraphy* **2018**, *15*, 1–20. [\[CrossRef\]](#)
67. Dott, J.R.H. The Importance of Eolian Abrasion in Supermature Quartz Sandstones and the Paradox of Weathering on Vegetation-Free Landscapes. *J. Geol.* **2003**, *111*, 387–405. [\[CrossRef\]](#)
68. Folk, R.L. Bimodal supermature sandstones: Product of the desert floor. In Proceedings of the 23rd International Geological Congress, Prague, Czechoslovakia, 19–28 August 1968; Volume 9, pp. 9–32.
69. Haynes, J.T.; Melson, W.G.; O’Hearn, T.; Goggin, K.E.; Hubbell, R. A High Potassium Mid-Ordovician Shale of the Central Appalachian Foredeep: Implications for Reconstructing Taconian Explosive Volcanism. *Shales Mudstones* **1998**, *2*, 129–141.
70. Haynes, J.T.; Durst, T.R.; Fichter, L.S. Petrographic similarities between framework grains in Ordovician arenites from the Blount and Queenston molasse of the Taconic orogeny, Virginia Appalachians. In *Geological Society of America Abstracts with Programs*; Geological Society of America: Boulder, CO, USA, 2015; Volume 47, p. 21.
71. Clift, P.D.; Lin, A.T.S.; Carter, A.; Wu, F.; Draut, A.E.; Lai, T.-H.; Fei, L.-Y.; Schouten, H.; Teng, L.S. Post-collisional collapse in the wake of migrating arc-continent collision in the Ilan Basin, Taiwan. In *Formation and Applications of the Sedimentary Record in Arc Collision Zones*; Draut, A.E., Clift, P.D., Scholl, D.W., Eds.; Geological Society of America: Boulder, CO, USA, 2008; Volume 436, pp. 257–278.
72. Burbank, D.W.; Beck, R.A.; Reynolds, R.G.H.; Hobbs, R.; Tahirkheli, R.A.K. Thrusting and gravel progradation in foreland basins: A test of post-thrusting gravel dispersal. *Geology* **1988**, *16*, 1143–1146. [\[CrossRef\]](#)
73. Burbank, D.W.; Beck, R.A.; Mulder, T.; Yin, A.; Harrison, T. The Himalayan foreland basin. *World Reg. Geol.* **1996**, 149–190.
74. Burbank, D.W. Causes of recent Himalayan uplift deduced from deposited patterns in the Ganges basin. *Nature* **1992**, *357*, 680–683. [\[CrossRef\]](#)
75. Shanmugam, G.; Benedict, G.L. Fine-grained carbonate debris flow, Ordovician basin margin, southern Appalachians. *J. Sediment. Res.* **1978**, *48*, 1233–1239. [\[CrossRef\]](#)
76. Diecchio, R.J. Post-Martinsburg Ordovician stratigraphy of Virginia and West Virginia. *Va. Div. Miner. Resour. Publ.* **1985**, *57*, 77.
77. Etensohn, F.R. Modeling the nature and development of major paleozoic clastic wedges in the Appalachian Basin, USA. *J. Geodyn.* **2004**, *37*, 657–681. [\[CrossRef\]](#)
78. Yin, A. Cenozoic tectonic evolution of the Himalayan orogen as constrained by along-strike variation of structural geometry, exhumation history, and foreland sedimentation. *Earth-Sci. Rev.* **2006**, *76*, 1–131. [\[CrossRef\]](#)
79. Clift, P.D.; Carter, A.; Krol, M.; Kirby, E. Constraints on India-Eurasia collision in the Arabian Sea region taken from the Indus Group, Ladakh Himalaya, India. *Geol. Soc. Lond. Spec. Publ.* **2002**, *195*, 97–116. [\[CrossRef\]](#)
80. Clift, P.D.; Shimizu, N.; Layne, G.; Blusztajn, J.; Gaedicke, C.; Schluter, H.-U.; Clark, M.; Amjad, S. Development of the Indus Fan and its significance for the erosional history of the Western Himalaya and Karakoram. *Geol. Soc. Am. Bull.* **2001**, *113*, 1039–1051. [\[CrossRef\]](#)
81. Männik, P.; Lehnert, O.; Nõlvak, J.; Joachimski, M.M. Climate changes in the pre-Hirnantian Late Ordovician based on  $\delta^{18}\text{O}$  studies from Estonia. *Palaeogeogr. Palaeoclimatol. Palaeoecol.* **2021**, *569*, 110347. [\[CrossRef\]](#)
82. Herrmann, A.D.; Macleod, K.G.; Leslie, S.A. Did a Volcanic Mega-Eruption Cause Global Cooling during the Late Ordovician? *Palaios* **2010**, *25*, 831–836. [\[CrossRef\]](#)
83. Kellberg, J.M.; Grant, L.F. Coarse Conglomerates of the Middle Ordovician in the Southern Appalachian Valley. *Geol. Soc. Am. Bull.* **1956**, *67*, 697–716. [\[CrossRef\]](#)
84. Shanmugam, G.; Walker, K.R. Sedimentation, subsidence, and evolution of a foredeep basin in the Middle Ordovician, southern Appalachians. *Am. J. Sci.* **1980**, *280*, 479–496. [\[CrossRef\]](#)
85. Shanmugam, G.; Walker, K.R. Tectonic significance of distal turbidites in the Middle Ordovician Blockhouse and lower Sevier formations in East Tennessee. *Am. J. Sci.* **1978**, *278*, 551–578. [\[CrossRef\]](#)
86. Shanmugam, G.; Walker, K.R. Anatomy of the middle ordovician sevier shale basin, eastern Tennessee. *Sediment. Geol.* **1983**, *34*, 315–337. [\[CrossRef\]](#)
87. Pope, M.; Read, J.F. High-Resolution Surface and Subsurface Sequence Stratigraphy of Late Middle to Late Ordovician (Late Mohawkian-Cincinnatian) Foreland Basin Rocks, Kentucky and Virginia. *AAPG Bull.* **1997**, *81*, 1866–1893. [\[CrossRef\]](#)

88. Leslie, S.A.; Bergström, S.M. Revision of the North American late Middle Ordovician standard stage classification and timing of the Trenton transgression based on K-bentonite bed correlation. In *Ordovician Odyssey: Short Papers for the Seventh International Symposium on the Ordovician System*; Cooper, J.D., Ed.; Pacific Section of the Society for Sedimentary Geologists (SEPM): Broken Arrow, OK, USA, 1995; Volume 77, pp. 49–54.
89. Leslie, S.A.; Bergström, S.M. Use of K-bentonite beds as time-planes for high-resolution lithofacies analysis and assessment of net rock accumulation rate: An example from the upper Middle Ordovician of eastern North America. In *Paleozoic Sequence Stratigraphy, Biostratigraphy, and Biogeography: Studies in Honor of J. Granville ("Jess") Johnson*; Geological Society of America Special Paper 321; Klapper, G., Murphy, M.A., Talent, J.A., Eds.; Geological Society of America: Boulder, CO, USA, 1997; pp. 11–21.
90. Garzanti, E. The Himalayan Foreland Basin from collision onset to the present: A sedimentary-petrology perspective. *Geol. Soc. Lond. Spec. Publ.* **2019**, *483*, 65–122. [[CrossRef](#)]
91. Blair, T.C.; Bilodeau, W.L. Development of tectonic cyclothems in rift, pull-apart, and foreland basins: Sedimentary response to episodic tectonism. *Geology* **1988**, *16*, 517–520. [[CrossRef](#)]
92. van Ufford, A.Q.; Cloos, M. Cenozoic tectonics of New Guinea. *AAPG Bull.* **2005**, *89*, 119–140. [[CrossRef](#)]
93. Cloos, M.; Sapiie, B.; van Ufford, A.Q.; Weiland, R.J.; Warren, P.Q.; McMahon, T.P. *Collisional Delamination in New Guinea: The Geotectonics of Subducting Slab Breakoff*; Geological Society of America Special Papers; Geological Society of America: Boulder, CO, USA, 2005; Volume 400, pp. 1–51.
94. Chandler, F.W. Quartz arenites: Review and interpretation. *Sediment. Geol.* **1988**, *58*, 105–126. [[CrossRef](#)]
95. Suttner, L.J.; Basu, A.; Mack, G.H. Climate and the origin of quartz arenites. *J. Sediment. Res.* **1981**, *51*, 1235–1246.
96. Heller, P.L.; Angevine, C.L.; Winslow, N.S.; Paola, C. Two-phase stratigraphic model of foreland-basin sequences. *Geology* **1988**, *16*, 501–504. [[CrossRef](#)]
97. Avigad, D.; Sandler, A.; Kolodner, K.; Stern, R.J.; McWilliams, M.; Miller, N.; Beyth, M. Mass-production of Cambro–Ordovician quartz-rich sandstone as a consequence of chemical weathering of Pan-African terranes: Environmental implications. *Earth Planet. Sci. Lett.* **2005**, *240*, 818–826. [[CrossRef](#)]
98. Johnsson, M.J.; Stallard, R.F.; Meade, R.H. First-Cycle Quartz Arenites in the Orinoco River Basin, Venezuela and Colombia. *J. Geol.* **1988**, *96*, 263–277. [[CrossRef](#)]
99. Potter, P.E. Petrology and chemistry of modern big river sands. *J. Geol.* **1978**, *86*, 423–449. [[CrossRef](#)]
100. Kump, L.R.; Arthur, M.A.; Patzkowsky, M.E.; Gibbs, M.T.; Pinkus, D.S.; Sheehan, P.M. A weathering hypothesis for glaciation at high atmospheric pCO<sub>2</sub> during the Late Ordovician. *Palaeogeogr. Palaeoclimatol. Palaeoecol.* **1999**, *152*, 173–187. [[CrossRef](#)]
101. Young, S.A.; Saltzman, M.R.; Bergström, S.M. Upper Ordovician (Mohawkian) carbon isotope ( $\delta^{13}\text{C}$ ) stratigraphy in eastern and central North America: Regional expression of a perturbation of the global carbon cycle. *Palaeogeogr. Palaeoclimatol. Palaeoecol.* **2005**, *222*, 53–76. [[CrossRef](#)]
102. Herrmann, A.D.; Leslie, S.A.; MacLeod, K.G. Did intense volcanism trigger the first Late Ordovician icehouse?: COMMENT. *Geology* **2011**, *39*, e237. [[CrossRef](#)]
103. Quinton, P.C.; Law, S.; Macleod, K.G.; Herrmann, A.D.; Haynes, J.T.; Leslie, S.A. Testing the early Late Ordovician cool-water hypothesis with oxygen isotopes from conodont apatite. *Geol. Mag.* **2017**, *155*, 1727–1741. [[CrossRef](#)]
104. Rosenau, N.A.; Herrmann, A.D.; Leslie, S.A. Conodont apatite  $\delta^{18}\text{O}$  values from a platform margin setting, Oklahoma, USA: Implications for initiation of Late Ordovician icehouse conditions. *Palaeogeogr. Palaeoclimatol. Palaeoecol.* **2012**, *315–316*, 172–180. [[CrossRef](#)]
105. Wright, Z.A.; Quinton, P.C.; Martin, E.E.; Leslie, S.A.; MacLeod, K.G.; Herrmann, A.D. Neodymium isotope ratios and a positive  $\delta^{13}\text{C}$  excursion: Interpreting the connection between oceanographic and climate changes during the early Late Ordovician of Laurentia. *Stratigraphy* **2017**, *14*, 443–456. [[CrossRef](#)]
106. Swanson-Hysell, N.L.; Macdonald, F.A. Tropical weathering of the Taconic orogeny as a driver for Ordovician cooling. *Geology* **2017**, *45*, 719–722. [[CrossRef](#)]
107. Herrmann, A.D.; Haupt, B.J.; Patzkowsky, M.E.; Seidov, D.; Slingerland, R.L. Response of Late Ordovician paleoceanography to changes in sea level, continental drift, and atmospheric pCO<sub>2</sub>: Potential causes for long-term cooling and glaciation. *Palaeogeogr. Palaeoclimatol. Palaeoecol.* **2004**, *210*, 385–401. [[CrossRef](#)]
108. Herrmann, A.D.; Haupt, B. Toward identifying potential causes for stratigraphic change in subtropical to tropical Laurentia during the Mohawkian (early Late Ordovician). In *The Ordovician Earth System*; Finney, S.C., Berry, W.B.N., Eds.; The Geological Society of America Special Paper 466; Geological Society of America: Boulder, CO, USA, 2010; pp. 29–35.
109. Pohl, A.; Donnadieu, Y.; Le Hir, G.; Buoncristiani, J.F.; Vennin, E. Effect of the Ordovician paleogeography on the (in)stability of the climate. *Clim. Past* **2014**, *10*, 2053–2066. [[CrossRef](#)]
110. Avigad, D.; Kolodner, K.; McWilliams, M.; Persing, H.; Weissbrod, T. Origin of northern Gondwana Cambrian sandstone revealed by detrital zircon SHRIMP dating. *Geology* **2003**, *31*, 227–230. [[CrossRef](#)]
111. Kolodner, K.; Avigad, D.; McWilliams, M.; Wooden, J.L.; Weissbrod, T.; Feinstein, S. Provenance of north Gondwana Cambrian–Ordovician sandstone: U–Pb SHRIMP dating of detrital zircons from Israel and Jordan. *Geol. Mag.* **2006**, *143*, 367–391. [[CrossRef](#)]
112. Johnsson, M.J.; Stallard, R.F.; Lundberg, N. Controls on the composition of fluvial sands from a tropical weathering environment: Sands of the Orinoco River drainage basin, Venezuela and Colombia. *Geol. Soc. Am. Bull.* **1991**, *103*, 1622–1647. [[CrossRef](#)]

113. Bayona, G. Controls on Middle to Late Ordovician Synorogenic Deposition in the Southeastern Corner of Laurentia. Ph.D. Dissertation, University of Kentucky, Lexington, KY, USA, 2003.
114. Bayona, G.; Thomas, W.A. Influence of pre-existing plate-margin structures on foredeep filling: Insights from the Taconian (Blountian) clastic wedge, Southeastern USA. *Sediment. Geol.* **2006**, *191*, 115–133. [[CrossRef](#)]
115. Hughes, G.R.; Mahood, G.A. Tectonic controls on the nature of large silicic calderas in volcanic arcs. *Geology* **2008**, *36*, 627–630. [[CrossRef](#)]
116. Thomas, W.A. Genetic relationship of rift-stage crustal structure, terrane accretion, and foreland tectonics along the southern Appalachian-Ouachita orogen. *J. Geodyn.* **2004**, *37*, 549–563. [[CrossRef](#)]
117. Whisner, S.C. The Middle Ordovician Tellico-Sevier Syncline: A Stratigraphic, Structural, and Paleoseismic Investigation. Ph.D. Dissertation, University of Tennessee, Knoxville, TN, USA, 2005.
118. Hamilton, W. *Tectonics of the Indonesian Region*; U.S. Government Publishing Office: Washington, DC, USA, 1979.
119. Curray, J.R. The Sunda Arc: A model for oblique plate convergence. *Neth. J. Sea Res.* **1989**, *24*, 131–140. [[CrossRef](#)]
120. Pigram, C.J.; Davies, P.J.; Feary, D.A.; Symonds, P.A. Tectonic controls on carbonate platform evolution in southern Papua New Guinea: Passive margin to foreland basin. *Geology* **1989**, *17*(3), 199–202. [[CrossRef](#)]
121. Davies, H.L. The geology of New Guinea—The cordilleran margin of the Australian continent. *Episodes* **2012**, *35*, 87–102. [[CrossRef](#)]
122. Baldwin, S.L.; Fitzgerald, P.G.; Webb, L.E. Tectonics of the New Guinea Region. *Annu. Rev. Earth Planet. Sci.* **2012**, *40*, 495–520. [[CrossRef](#)]
123. Large, S.J.E.; Quadt, A.v.; Wotzlaw, J.-F.; Guillong, M.; Heinrich, C.A. Magma Evolution Leading to Porphyry Au-Cu Mineralization at the Ok Tedi Deposit, Papua New Guinea: Trace Element Geochemistry and High-Precision Geochronology of Igneous Zircon. *Econ. Geol.* **2018**, *113*, 39–61. [[CrossRef](#)]
124. Holm, R.J.; Spandler, C.; Richards, S.W. Continental collision, orogenesis and arc magmatism of the Miocene Maramuni arc, Papua New Guinea. *Gondwana Res.* **2015**, *28*, 1117–1136. [[CrossRef](#)]
125. Baldwin, B.; Butler, J.R. Hamilton's Indonesia Map and the Appalachian Mountain System. *J. Geol. Educ.* **1982**, *30*, 93–96. [[CrossRef](#)]
126. Decker, J.; Ferdian, F.; Morton, A.; Fanning, M.; White, L.T. New geochronology data from eastern Indonesia—An aid to understanding sedimentary provenance in a frontier region. In Proceedings of the Indonesian Petroleum Association 41st Annual Convention & Exhibition IPA17-551-G, Central Jakarta, Indonesia, 17–19 May 2017.
127. Nash, C.R.; Artmont, G.; Gillan, M.L.; Lennie, D.; O'Connor, G.; Parris, K.R. Structure of the Irian Jaya Mobile Belt, Irian Jaya, Indonesia. *Tectonics* **1993**, *12*, 519–535. [[CrossRef](#)]
128. Van Wyck, N.; Williams, I.S. Age and provenance of basement metasediments from the Kubor and Bena Bena Blocks, central Highlands, Papua New Guinea: Constraints on the tectonic evolution of the northern Australian cratonic margin. *Aust. J. Earth Sci.* **2002**, *49*, 565–577. [[CrossRef](#)]
129. Munroe, S.M.; Williams, I.S. The Archaean basement of Papua New Guinea: Evidence from the Porgera intrusive complex. *Geol. Soc. Aust. Abstr.* **1996**, *41*, 308.
130. Zimmermann, S.; Hall, R. Provenance of Cretaceous sandstones in the Banda Arc and their tectonic significance. *Gondwana Res.* **2019**, *67*, 1–20. [[CrossRef](#)]
131. Smith, V.C.; Pearce, N.J.G.; Matthews, N.E.; Westgate, J.A.; Petraglia, M.D.; Haslam, M.; Lane, C.S.; Korisettar, R.; Pal, J.N. Geochemical fingerprinting of the widespread Toba tephra using biotite compositions. *Quat. Int.* **2011**, *246*, 97–104. [[CrossRef](#)]
132. Chesner, C.A. The Toba Caldera Complex. *Quat. Int.* **2012**, *258*, 5–18. [[CrossRef](#)]
133. Haynes, J.T.; Melson, W.G.; Goggin, K.E. Biotite phenocryst composition shows that the two K-bentonites in the Little Oak Limestone (Ordovician) at the Old North Ragland quarry, Alabama, are the same structurally repeated tephra layer. *Southeast. Geol.* **1996**, *36*, 85–98.
134. Haynes, J.T.; Huff, W.D.; Melson, W.G. Major Ordovician tephra generated by caldera forming explosive volcanism on continental crust: Evidence from biotite compositions. In *Ordovician of the World: Cuadernos del Museo Geominero*; Gutierrez-Marco, J.C., Rabano, I., Garcia-Bellido, D., Eds.; Instituto Geologico y Minero de Espana: Madrid, Spain, 2011; pp. 229–235.
135. Gregg, P.M.; de Silva, S.L.; Grosfils, E.B.; Parmigiani, J.P. Catastrophic caldera-forming eruptions: Thermomechanics and implications for eruption triggering and maximum caldera dimensions on Earth. *J. Volcanol. Geotherm. Res.* **2012**, *241–242*, 1–12. [[CrossRef](#)]
136. Grocke, S.B.; de Silva, S.L.; Iriarte, R.; Lindsay, J.M.; Cottrell, E. Catastrophic Caldera-Forming (CCF) Monotonous Silicic Magma Reservoirs: Geochemical and Petrological Constraints on Heterogeneity, Magma Dynamics, and Eruption Dynamics of the 3–49 Ma Tara Supereruption, Guacha II Caldera, SW Bolivia. *J. Petrol.* **2017**, *58*, 227–260. [[CrossRef](#)]
137. Draut, A.E.; Clift, P.D.; Hannigan, R.E.; Layne, G.; Shimizu, N. A model for continental crust genesis by arc accretion: Rare earth element evidence from the Irish Caledonides. *Earth Planet. Sci. Lett.* **2002**, *203*, 861–877. [[CrossRef](#)]

**Disclaimer/Publisher's Note:** The statements, opinions and data contained in all publications are solely those of the individual author(s) and contributor(s) and not of MDPI and/or the editor(s). MDPI and/or the editor(s) disclaim responsibility for any injury to people or property resulting from any ideas, methods, instructions or products referred to in the content.